

Migraine-Associated Mutation in the Na,K-ATPase Leads to Disturbances in Cardiac Metabolism and Reduced Cardiac Function

Staehr, Christian; Rohde, Palle Duun; Krarup, Nikolaj Thure; Ringgaard, Steffen; Laustsen, Christoffer; Johnsen, Jacob; Nielsen, Rikke; Beck, Hans Christian; Morth, Jens Preben; Lykke-Hartmann, Karin; Jespersen, Nicholas Riise; Abramochkin, Denis; Nyegaard, Mette; Bøtker, Hans Erik; Aalkjaer, Christian; Matchkov, Vladimir

Published in:

Journal of the American Heart Association

DOI (link to publication from Publisher):

[10.1161/JAHA.121.021814](https://doi.org/10.1161/JAHA.121.021814)

Creative Commons License

CC BY-NC 4.0

Publication date:

2022

Document Version

Publisher's PDF, also known as Version of record

[Link to publication from Aalborg University](#)

Citation for published version (APA):

Staehr, C., Rohde, P. D., Krarup, N. T., Ringgaard, S., Laustsen, C., Johnsen, J., Nielsen, R., Beck, H. C., Morth, J. P., Lykke-Hartmann, K., Jespersen, N. R., Abramochkin, D., Nyegaard, M., Bøtker, H. E., Aalkjaer, C., & Matchkov, V. (2022). Migraine-Associated Mutation in the Na,K-ATPase Leads to Disturbances in Cardiac Metabolism and Reduced Cardiac Function. *Journal of the American Heart Association*, 11(7), Article e021814. <https://doi.org/10.1161/JAHA.121.021814>

General rights

Copyright and moral rights for the publications made accessible in the public portal are retained by the authors and/or other copyright owners and it is a condition of accessing publications that users recognise and abide by the legal requirements associated with these rights.

- Users may download and print one copy of any publication from the public portal for the purpose of private study or research.
- You may not further distribute the material or use it for any profit-making activity or commercial gain
- You may freely distribute the URL identifying the publication in the public portal -


Take down policy

If you believe that this document breaches copyright please contact us at vbn@aub.aau.dk providing details, and we will remove access to the work immediately and investigate your claim.

Downloaded from vbn.aau.dk on: December 06, 2025

ORIGINAL RESEARCH

Migraine-Associated Mutation in the Na,K-ATPase Leads to Disturbances in Cardiac Metabolism and Reduced Cardiac Function

Christian Staehr , MD; Palle Duun Rohde , PhD; Nikolaj Thure Krarup , PhD; Steffen Ringgaard , PhD; Christoffer Laustsen , PhD; Jacob Johnsen, PhD; Rikke Nielsen , PhD; Hans Christian Beck , PhD; Jens Preben Morth , PhD; Karin Lykke-Hartmann , PhD; Nichlas Riise Jespersen , PhD; Denis Abramochkin , PhD; Mette Nyegaard , PhD; Hans Erik Bøtke , DMS; Christian Aalkjaer, DMS; Vladimir Matchkov , DMS

BACKGROUND: Mutations in *ATP1A2* gene encoding the Na,K-ATPase α_2 isoform are associated with familial hemiplegic migraine type 2. Migraine with aura is a known risk factor for heart disease. The Na,K-ATPase is important for cardiac function, but its role for heart disease remains unknown. We hypothesized that *ATP1A2* is a susceptibility gene for heart disease and aimed to assess the underlying disease mechanism.

METHODS AND RESULTS: Mice heterozygous for the familial hemiplegic migraine type 2-associated G301R mutation in the *Atp1a2* gene ($\alpha_2^{+/G301R}$ mice) and matching wild-type controls were compared. Reduced expression of the Na,K-ATPase α_2 isoform and increased expression of the α_1 isoform were observed in hearts from $\alpha_2^{+/G301R}$ mice (Western blot). Left ventricular dilation and reduced ejection fraction were shown in hearts from 8-month-old $\alpha_2^{+/G301R}$ mice (cardiac magnetic resonance imaging), and this was associated with reduced nocturnal blood pressure (radiotelemetry). Cardiac function and blood pressure of 3-month-old $\alpha_2^{+/G301R}$ mice were similar to wild-type mice. Amplified Na,K-ATPase-dependent Src kinase/Ras/Erk1/2 (p44/42 mitogen-activated protein kinase) signaling was observed in hearts from 8-month-old $\alpha_2^{+/G301R}$ mice, and this was associated with mitochondrial uncoupling (respirometry), increased oxidative stress (malondialdehyde measurements), and a heart failure-associated metabolic shift (hyperpolarized magnetic resonance). Mitochondrial membrane potential (5,5',6,6'-tetrachloro-1,1',3,3'-tetraethylbenzimidazolcarbocyanine iodide dye assay) and mitochondrial ultrastructure (transmission electron microscopy) were similar between the groups. Proteomics of heart tissue further suggested amplified Src/Ras/Erk1/2 signaling and increased oxidative stress and provided the molecular basis for systolic dysfunction in 8-month-old $\alpha_2^{+/G301R}$ mice.

CONCLUSIONS: Our findings suggest that *ATP1A2* mutation leads to disturbed cardiac metabolism and reduced cardiac function mediated via Na,K-ATPase-dependent reactive oxygen species signaling through the Src/Ras/Erk1/2 pathway.

Key Words: heart failure ■ migraine ■ mitochondrial function ■ Na,K-ATPase ■ oxidative stress

The Na,K-ATPase is an ion pump essential for maintaining sodium and potassium ion gradients across the plasma membrane in all mammalian cells. In the cardiomyocyte membrane, several catalytic α subunits of the Na,K-ATPase have distinct subcellular localizations^{1,2} and are suggested to serve

different cell functions.^{3–5} It has been proposed that the α_2 isoform is localized mainly in transverse tubules at the junctions with the sarcoplasmic reticulum, whereas the quantitatively prevalent α_1 isoform is ubiquitously distributed in the plasma membrane of cardiomyocytes.^{1,2,4} The α_1 isoform Na,K-ATPase was

Correspondence to: Christian Staehr, MD, Department of Biomedicine, Aarhus University, Høegh-Guldbergs Gade 10, DK-8000 Aarhus C, Denmark.
E-mail: chst@biomed.au.dk

Supplemental Material is available at <https://www.ahajournals.org/doi/suppl/10.1161/JAHA.121.021814>

For Sources of Funding and Disclosures, see page 18.

© 2022 The Authors. Published on behalf of the American Heart Association, Inc., by Wiley. This is an open access article under the terms of the Creative Commons Attribution-NonCommercial License, which permits use, distribution and reproduction in any medium, provided the original work is properly cited and is not used for commercial purposes.

JAHA is available at: www.ahajournals.org/journal/jaha

CLINICAL PERSPECTIVE

What Is New?

- Familial hemiplegic migraine-associated mutation of the Na,K-ATPase α_2 isoform, encoded by the *ATP1A2* gene, was associated with mitochondrial uncoupling and high levels of oxidative stress in the heart.
- The disturbances in cardiac metabolism were associated with dilation of the left ventricle and reduced ejection fraction in elderly mice carrying the mutation.
- Our data indicated that imbalanced Na,K-ATPase-dependent Src/Ras/Erk1/2 signaling in cardiomyocytes underlies mitochondrial uncoupling, leading to increased generation of reactive oxygen species.

What Are the Clinical Implications?

- Our finding of a link between a subtype of migraine and cardiac dysfunction provides important novel insight into the otherwise inexplicable comorbidity between migraine and cardiovascular disease.
- The *ATP1A2* gene may be considered a risk gene for cardiovascular disease.
- Our study suggests that monitoring and special attention to cardiovascular health are warranted in patients carrying migraine-associated *ATP1A2* missense variants.

Nonstandard Abbreviations and Acronyms

Erk1/2	p44/42 mitogen-activated protein kinase
FHM2	familial hemiplegic migraine type 2
IPA	ingenuity pathway analysis
PLCy	phospholipase Cy
JC-1	5,5',6,6'-tetrachloro-1,1',3,3'-tetraethylbenzimidazolocarbo-cyanine iodide
ROS	reactive oxygen species
WT	wild type

proposed to serve mainly a housekeeping role for intracellular ion homeostasis, whereas the α_2 isoform has been suggested to serve more specific regulatory functions.² Expressional changes in the Na,K-ATPase have dramatic consequences for cardiac function. A lineal correlation between left ventricular ejection fraction and the Na,K-ATPase content in the cardiac tissue has previously been shown.⁶ Accordingly, reduction in the Na,K-ATPase was reported in patients with heart

failure⁷ and dilated cardiomyopathy.⁸ Moreover, experimental models suggest the importance of the α_2 isoform Na,K-ATPase for cardiac pathology.^{4,5,9} Thus, global heterozygote knockout of the Na,K-ATPase α_2 isoform leads to cardiac hypercontractility attributable to increased intracellular Ca^{2+} transients.¹⁰ It has been proposed that the α_2 isoform modulates spatially restricted intracellular Na^+ concentrations¹¹ and consequently intracellular Ca^{2+} concentrations via interaction with the Na,Ca-exchanger.^{3,4,12} Intracellular Na^+ concentrations, controlled by Na^+ channels, $\text{Na}^+/\text{Ca}^{2+}$ exchange, and the Na,K-ATPase, are vital for preserving the electrical and contractile activity of the heart.¹³

In addition to controlling intracellular ion homeostasis, the Na,K-ATPase α isoforms are proposed to be implicated in ion transport-independent protein kinase signaling cascades,¹⁴ including the Na,K-ATPase–Src kinase signal transduction.¹⁵ Na,K-ATPase inhibition leads to activation of Src kinase. Increased activation of Src kinase in cardiomyocytes leads to initiation of downstream signaling pathways (ie, Src/Ras/Erk1/2 [p44/42 mitogen-activated protein kinase] and Src/phospholipase Cy [PLCy]/inositol trisphosphate-receptor signaling). The Src/Ras/Erk1/2 pathway is associated with mitochondrial generation of reactive oxygen species (ROS),¹⁶ whereas the Src/PLCy/inositol trisphosphate-receptor pathway is suggested to regulate intracellular Ca^{2+} homeostasis. These signaling pathways initiated from the cardiac Na,K-ATPase have previously been implicated in changes of cardiac morphology and function,^{17–20} including the Na,K-ATPase/ROS signaling playing a key role in experimental uremic cardiomyopathy.²¹ Inhibition of this signaling pathway ameliorates cardiomyopathic changes.²² Although many studies suggest an extraordinary significance of the Na,K-ATPase signaling, the specific signaling pathways involved in cardiac pathologies remain to be elucidated.

Mutation in the *ATP1A2* gene encoding the Na,K-ATPase α_2 isoform is associated with familial hemiplegic migraine type 2 (FHM2; OMIM No. 602481), a severe form of migraine with aura.²³ Nationwide population-based cohort studies have recently characterized migraine, particularly migraine with aura, as a significant risk factor for development of cardiovascular disease.²⁴ We hypothesized that the FHM2-associated mutation of the Na,K-ATPase α_2 isoform leads to heart disease caused by mitochondrial dysfunction and oxidative stress as a consequence of changed protein kinase signaling pathways downstream from the Na,K-ATPase and aimed to characterize the involved signaling.

We tested our hypothesis in heterozygous mice carrying the G301R mutation in the *Atp1a2* gene²⁵ (Figure S1), which is associated with a severe phenotype in patients with FHM2.²⁶ The $\alpha_2^{+/G301R}$ mouse model was

previously shown to phenocopy FHM2-relevant disease traits (ie, neuropsychiatric²⁵ and cerebrovascular^{27,28} manifestations). We compared cardiac function in 3- and 8-month-old $\alpha_2^{+/G301R}$ mice with age-matched wild-type (WT) controls, addressing a progression of the pathology associated with decreased cardiac expression of the Na,K-ATPase α_2 isoform. The functional analyses in vivo (ie, cardiac magnetic resonance imaging with and without hyperpolarization and radiotelemetry) and ex vivo (respirometry, membrane potential measurements, and transmission electron microscopy) were further strengthened by expressional and biochemical measurements as well as proteomics of heart samples. The results of this study provide mechanistic insight into how FHM2-associated mutation in the Na,K-ATPase α_2 isoform may lead to increased risk of heart failure and cardiomyopathy-like changes.

METHODS

The data that support the findings of this study are available from the corresponding author on reasonable request.

All procedures were performed according to the guidelines from Directive 2010/63/EU of the European Parliament on the protection of animals used for scientific purposes. The experiments were approved by and conducted with permission from the Animal Experiments Inspectorate of the Danish Ministry of Environment and Food (No. 2016-15-0201-00982). Animal experiments were reported in accordance with the Animal Research: Reporting in Vivo Experiments guidelines.

The $\alpha_2^{+/G301R}$ mice were generated and bred, as described previously.^{25,27} Mice were housed under a 12:12 light/dark cycle, and food and water were provided ad libitum. Approximately 3- and 8-month-old heterozygous $\alpha_2^{+/G301R}$ mice (homozygous pups died immediately after birth) were used in the current study. A previous study found sex-coupled differences in behavioural tests.²⁵ Consequently, we included an equal number of males and females. However, as no sex-coupled difference was observed, data from males and females were pooled.

Western Blot Protein Semiquantification in Left Ventricle Tissue

Mice were euthanized by cervical dislocation, and the hearts were dissected into ice-cold physiological salt solution (in mmol/L: NaCl 115.8, KCl 2.82, KH_2PO_4 1.18, MgSO_4 1.2, NaHCO_3 25, CaCl_2 1.6, EDTA 0.03, and glucose 5.5, gassed with 5% CO_2 in air and adjusted to pH 7.4), blotted dry, and weighed. In the experiments where maximal capacity of ouabain-dependent signaling was assessed, the

dissected left ventricles were equilibrated for 1 hour in physiological salt solution gassed with 5% CO_2 in air at 37 °C, and then, incubated for 30 minutes with 1 mmol/L ouabain.

Left ventricles were snap frozen in liquid N_2 for later storage at -80 °C. Left ventricles were lysed in lysis buffer (in mmol/L: Tris-HCl 10, sucrose 250, EDTA 1, EGTA 1, and Triton X-100 2%, pH 7.4; and 1 tablet protease inhibitor per 10 mL) and centrifuged at 10 000g. Total protein concentrations in the supernatants were measured using BCA Protein Assay Kit (ThermoFisher Scientific, Waltham, MA). A total of 10 μg of total protein diluted in Laemmli sample buffer (Bio-Rad, Hercules, CA) was loaded onto 4% to 20% precast polyacrylamide stain-free gels (Criterion TGX Stain-free precast gel; Bio-Rad). Total protein load was detected on the stain-free gels using UV light in imaging system (c600; Azur Biosystems, Dublin, CA).

The proteins were electrotransferred onto membranes that were then blocked by an incubation in 5% BSA and 5% nonfat dry milk in PBS with 0.5% vol/vol Tween 20. To detect PLC γ , Src, and Erk1/2, the membranes were divided before incubation with the antibodies into 2 parts; the upper part, above 75 kDa, was used to detect PLC γ and p-PLC γ ; and the lower part, below 75 kDa, was used to detect either Src and p-Src or Erk1/2 and p-Erk1/2, respectively. The membranes were then incubated overnight at 4 °C with the following antibodies:

- α_1 Isoform Na,K-ATPase antibody (1:2000; No. NB2-61137H; Novus Biologicals Inc, Centennial, CO).
- Antibody against the α_2 isoform Na,K-ATPase (1:2000; No. AB9094; Chemicon, Burlington, MA).
- Antibody against the Na,Ca-exchanger-1 (1:200; No. ANX-011; Alomone Labs, Israel).
- Antibody against total cSrc (1:500; sc-8056; Santa Cruz Biotechnology Inc, Dallas, TX) or antibody against cSrc phosphorylated at pY418 (1:200; No. 44660G; ThermoFisher Scientific).
- Antibody against total Erk1/2 (1:3000; No. CST4696; Cell Signaling Technology, Inc, Danvers, MA) or antibody against Erk1/2 phosphorylated at Thr202/Tyr204 (1:2000; No. CST9101; Cell Signaling Technology, Inc).
- Antibody against total PLC γ (1:3000; No. CST2822; Cell Signaling Technology, Inc) or antibody against PLC γ phosphorylated at Tyr783 (1:3000; No. CST2821; Cell Signaling Technology, Inc).

After intensive washing, the membranes were incubated with horseradish peroxidase-conjugated secondary antibody (1:4000; Dako, Denmark) for 1 hour in PBS with 0.5% vol/vol Tween 20. Excess antibody was removed by washing, and bound antibody was

detected by an enhanced chemiluminescence kit (ECL, Amersham, UK). Detected protein was normalized using the ImageJ program (National Institutes of Health) as a ratio to total protein load measured in the membrane for the same probe, and expressed either as an absolute expression level or as a relative level of phosphorylated form over the total expression level of enzyme.

Mitochondrial Membrane Potential in Left Ventricles

Mice were euthanized by cervical dislocation, and the hearts were dissected into ice-cold physiological salt solution, as described above. Left ventricles were sliced at the level of the papillary muscle into 160- μ m slices using vibratome (1200 seconds; Leica Biosystems, Germany). The slices were incubated in 5,5',6,6'-tetrachloro-1,1',3,3'-tetraethylbenzimidazolcarbocyanine iodide (JC-1) solution prepared in accordance with the manufacturer manual (JC-1 mitochondria Staining Kit; catalog No. CS0390; Sigma-Aldrich, St. Louis, MO) for 15 minutes at 4 °C. To access the specificity of fluorescence from JC-1 aggregates in the polarized mitochondrial membrane, some left ventricle slices were incubated with JC-1 solution supplied with 1 μ mol/L valinomycin, a mitochondrial K⁺ ionophore that eliminate mitochondrial membrane potential.

JC-1 has a potential-sensitive shift in the emitted wavelength attributable to formation of red fluorescent J-aggregates in the polarized mitochondrial membrane.²⁹ JC-1 in its monomeric cytoplasmic form emits green light, whereas JC-1 in its aggregated form in the mitochondrial membrane emits red light. We placed JC-1 loaded slices on the confocal microscope (Zeiss LSM 7 Pascal; Zeiss, Germany) and excited at 488 and 543 nm to visualize JC-1 monomers and aggregates, respectively. Emitted light from JC-1 monomer and aggregate was collected at 499 to 545 nm and 579 to 651 nm, respectively. Mitochondrial membrane potential was estimated as red (579–651 nm)/green (499–545 nm) fluorescence ratio.²⁹

Cardiac Magnetic Resonance Imaging

Time-resolved magnetic resonance imaging (CINE scanning) assessed cardiac contractility and ventricular geometry. Cardiac magnetic resonance imaging was performed using an Agilent 9.4-T magnetic resonance imaging system (Santa Clara, CA) with a 40-mm millipede coil. During the experiment, mice were anesthetized by continuous ventilation with 1.8% sevoflurane (AbbVie, North Chicago, IL). To synchronize data acquisition, an integrated subcutaneous 3-electrode ECG was used in combination with a respiration-sensing device (Small Animal Instruments, Inc, New York, NY). The body temperature was kept at 37°C with a warm-air heating system connected to a rectal probe. ECG, respiration

rate, and temperature were recorded in PC-SAM32 software (Small Animal Instruments, Inc).

Image variables for short-axis scans were as follows: flip angle, 15°; and 31 to 38 phases for 1 cardiac cycle, depending on heart rate. Field of view was 40×40 mm, and matrix was set to 192×192 pixels, resulting in pixel size of 0.21×0.21 mm². Eight slices with a thickness of 1.2 mm were acquired to cover the entire right and left ventricles. Two long-axis images were obtained, 4-chamber view and 2-chamber view, respectively. From the short-axis images, left ventricular myocardial mass was assessed by manual measurement of endocardial and epicardial borders on each slice. The short-axis images were also used to quantify end-diastolic and end-systolic volume of both ventricles that was used to calculate ejection fraction, stroke volume, cardiac output, and cardiac index. The analysis was done blinded using custom-made software.

Cardiac Magnetic Resonance With Hyperpolarization

Hyperpolarized [1-¹³C]pyruvate magnetic resonance scans were performed in the same 9.4-T preclinical magnetic resonance system equipped with a dual-tuned 4-mm ¹³C/¹H volume mouse coil (Rapid Biomedical, Rimpur, Germany). For each experiment, a sample of 127 mg of [1-¹³C]pyruvic acid mixed with 15 mmol/L AH111501 was polarized in a SPINALIGNER (Polarize IVS, Copenhagen, Denmark) polarizer for >1.5 hours at 6.7 T at 1.3 K, to ensure a reproducible polarization of 50% on average, similar to previous reports in the SPINLAB polarizer.³⁰ Each mouse received over 5 seconds an intravenous injection of 100 μ L per 25 g body weight of 125 mmol/L hyperpolarized [1-¹³C]-pyruvate. A slice-selective ¹³C spectroscopy-free induction decay sequence with a repetition time of 1 second, flip angle of 10°, and slice thickness of 10 mm covering the entire heart was used. The data were filtered with a zero shifted sine-bell function and a 15-Hz exponential line broadening, Fourier transformed and displayed in magnitude mode. The respective peaks were manually integrated using iNMR 6.1.4b (Nucleomatica, Molfetta, Italy). The area under the curve metabolite signal for [1-¹³C]lactate, [1-¹³C]alanine, and ¹³C-bicarbonate in the heart was normalized relative to the area under the curve [1-¹³C] pyruvate signal as a measure of conversion from pyruvate to metabolite.³¹

Telemetric Measurements of Blood Pressure and Heart Rate

Blood pressure was measured using radiotelemetry, as described previously.³² Mice were anesthetized by a combination of ketamine (SC 33 mg/100 g; Ketaminolvet; Intervet International, Boxmeer, the Netherlands) and xylazine (SC 7.5 mg/100 g; Narcoxylvet; Intervet

International) and placed on a thermostatically controlled warming platform to maintain body temperature at 37 °C. A midline incision through the shaved skin on the neck was made, and the mandibular glands were separated to access the carotid artery. The catheter of the radiotelemetry transmitter (PA-C10 and HD-X11; Data Sciences International, New Brighton, MN) was placed into the carotid artery, and the transmitter body was placed in a subcutaneous pocket. The skin incision was closed using 6-0 nonabsorbable suture. Analgesia was given subcutaneously at the end of the operation and again 12 hours after and 24 hours after the operation (0.2 mL/kg, buprenorphine hydrochloride, Temgesic; Schering-Plough Europe, Kenilworth, NJ). Mice were allowed to recover for at least 1 week before measurements were started. Telemetry signals were recorded at 256-Hz frequency in 10-second intervals each minute. Registration was performed with Dataquest A.R.T software 4.3 (Data Sciences International). Analyses were performed with Ponemah 8 (Data Sciences International). Arterial pressure was averaged at the time of minimal activity (between 12 AM and 2 PM) and at the time of maximal activity (between 8 PM and 10 PM).

Electrophysiological Characterization of Isolated Heart

Electrical activity in the isolated heart was measured, as described previously.³³ Mice were euthanized by cervical dislocation, and the hearts were rapidly excised. After dissection, the heart was immersed in an oxygenated physiological solution containing (in mmol/L): NaCl 130.0, KCl 5.6, NaH₂PO₄ 0.6, MgCl₂ 1.1, CaCl₂ 2, NaHCO₃ 20.0, and glucose 11.0, bubbled with carbogen (95% O₂ and 5% CO₂) with pH 7.4. The isolated hearts were pinned in the experimental chamber (3 mL) and superfused with physiological solution (10 mL/min; 37.5 °C). The hearts were cannulated through aorta and retrogradely perfused with constantly flowing solution of the same composition. The right auricle and right ventricular wall were opened to make endocardial surface within reach for microelectrode impalements.

Preparations were beating spontaneously in a stable rhythm generated by the sinoatrial node, throughout the experiment. After 30 minutes of equilibration in the perfusion chamber, transmembrane resting and action potentials were recorded from endocardial cardiomyocytes with sharp glass microelectrodes (30–45 MΩ) filled with mol/L KCl connected to a high input impedance amplifier model 1300 (A-M Systems, Sequim, WA). The signal was digitized and analyzed using specific software (L-card and DI-Soft, Moscow, Russia; and Synaptosoft, Decatur, GA). The measurements were done in 4 distinct regions: right atrial posterior part of intercaval region that contains sinoatrial node pacemaker area,³⁴ right atrial trabeculae, and right atrial and left ventricular wall.

Citrate Synthase Enzymatic Activity in Left Ventricle

Citrate synthase enzymatic activity in cardiac tissue homogenates was measured by spectrophotometry, as described previously,³⁵ and the results are expressed as μmol/min per g tissue. The cardiac tissue was homogenized in 1.5 mL of 0.3 mmol/L K₂HPO₄ with 0.05% BSA (pH 7.7). A total of 15 μL of 10% Triton X-100 was added, and samples were left on ice for 15 minutes. The homogenate was diluted 50 times in a solution containing (in mmol/L): 0.4 acetyl-CoA, 0.6 oxaloacetate, 0.157 5,5'-dithiobis-(2-nitrobenzoic acid), and 39 Tris-HCl (pH 8.0). The change of 5,5'-dithiobis-(2-nitrobenzoic acid) to 5-thiobis-(2-nitrobenzoic acid) at 37 °C was measured spectrophotometrically at 415 nm on an automatic analyser (Cobas 6000, C 501; Roche Diagnostics, Mannheim, Germany).

Respirometry of Left Ventricle

The 3- and 8-month-old mice were euthanized by cervical dislocation, and the left ventricle was quickly dissected and transferred to a biopsy preservation solution containing (in mmol/L): 10 Ca-EGTA buffer, 10⁻⁴ free Ca²⁺, 20 imidazole, 20 taurine, 50 K-MES, 0.5 dithiothreitol, 6.56 MgCl₂, 5.77 ATP, and 15 phosphocreatine, pH 7.1. The left ventricles were chemically permeabilized by incubation for 30 minutes in ice-cold biopsy preservation solution buffer containing 50 μg/mL saponin.³⁶ After washing twice for 10 minutes in an ice-cold respiration medium (MiRO5; in mmol/L: 110 sucrose, 60 K-lactobionate, 0.5 EGTA, 0.1% BSA, 3 MgCl₂, 20 taurine, 10 KH₂PO₄, and 20 HEPES; pH 7.1), ventricles were blotted dry and weighed.

Mitochondrial respiratory capacity was measured with high-resolution respirometry (Oxygraph-2k; Oroboros Instruments, Innsbruck, Austria) with nonfatty substrates.³⁶ All experiments were conducted at 37 °C in a hyperoxygenated environment (250–450 μmol/L) to preclude potential O₂ diffusion limitations. In the absence of adenylates, the basal respiration (ie, state 2 respiration supported by electron flow from complex I (glutamate and malate), was measured in the presence of 10 mmol/L glutamate and 2 mmol/L malate. The subsequent addition of 5 mmol/L ADP enables a coupled state 3 respiration supported by electron transfer from complex I (state 3 respiration with glutamate and malate). The whole data set was excluded, if the subsequent addition of 10 μmol/L cytochrome C (the test for integrity of the outer mitochondrial membrane) increased respiration by >10%.³⁷ The maximal coupled state 3 respiration in complex I and II was assessed with 10 mmol/L succinate. Oligomycin (2 μg/mL; eliminates ATP synthesis) was used to estimate proton leak across the inner mitochondrial membrane (ie, state 4_o of respiration). The residual O₂ consumption was measured in

the presence of 0.5 $\mu\text{mol/L}$ rotenone and 2.5 mmol/L antimycin A and serves as an indicator of uncoupled, nonmitochondrial respiration.³⁷

The steady-state respiratory rates were evaluated as an average oxygen consumption (O_2 in pmol/s) per milligram ventricle weight over the stable period of respiratory state using DatLab 6 software (Oroboros Instruments). The residual nonmitochondrial O_2 consumption was subtracted from all other values.

Lipid Peroxidation in Left Ventricle

Lipid peroxidation is commonly quantified by measuring the accumulating by-products (eg, malondialdehyde), as described previously.³⁸ Malondialdehyde is a common general product of nonenzymatic peroxidation of polyunsaturated fatty and arachidonic acids. The level of malondialdehyde was measured by thiobarbituric acid–reactive substances assay. Malondialdehyde in the sample was reacted with thiobarbituric acid to generate the malondialdehyde–thiobarbituric acid adduct. The malondialdehyde–thiobarbituric acid adduct was quantified colorimetrically at 532 nm.³⁸

Relative Protein Quantification in Left Ventricle Tissue Using 10-Plex Tandem Mass Tags

Left ventricles were dissected and lysed, as described above, for Western blot protocol. Proteins were isolated by acetone precipitation, redissolved in 0.2 mol/L triethylammonium bicarbonate, followed by reduction by dithiothreitol (5 mmol/L for 30 minutes at 50 °C), alkylation by iodoacetamide (15 mmol/L for 30 minutes at room temperature in the darkness), and proteolytic cleavage by the addition of trypsin in a 1:50 trypsin/protein ratio and overnight incubation at 37 °C. The resulting peptide samples were labeled with 2 sets of tandem mass tags from a 10-plex tandem mass tags set using the mass tags 127N, 127C, 128N, 128C, 129N, and 129C. A pool of all samples was labeled with mass tag 131 and served as reference channel. Tagged peptide samples were mixed in 2 sets of tagged peptide mixture, which each were subsequently fractionated by hydrophilic interaction chromatography and analyzed by reversed phase nanoliquid chromatography tandem mass spectrometry, as previously described.³⁹ In brief, the peptides were dissolved in hydrophilic interaction chromatography buffer B (90% [v/v] acetonitrile and 0.1% [v/v] trifluoroacetic acid) fractionated into 24 fractions using a Dionex UltiMate 3000 nano high-performance liquid chromatograph using a 42-minute linear gradient and a TSK gelamide-80 hydrophilic interaction chromatography column. Each fraction was then analyzed by reversed phase nanoliquid chromatography tandem mass spectrometry using a Dionex UltiMate 3000 nano high-performance liquid chromatograph coupled to a Q-exactive Orbitrap mass spectrometer, as

described.³⁹ The resulting Q-exactive raw data files were then processed and searched against the Uniprot mouse database using Proteome Discoverer version 2.1.0.81 (Thermo Scientific, Waltham, MA) integrated with the Sequest search engine and Mascot search engine (version 2.2.3) virtually, as previously described.³⁹ The mass spectrometry proteomics data have been deposited to the ProteomeXchange Consortium via the PRIDE⁴⁰ partner repository with the data set identifier PXD028952.

Ingenuity Pathway Analysis

Protein expression in the proteomics data from wild-type and $\alpha_2^{+/G301R}$ hearts was compared with unpaired *t*-test and uploaded into ingenuity pathway analysis (IPA) software (Qiagen, Redwood City, CA), where the differential protein expression was defined as $P < 0.05$ (Data S1). First, gene ontology pathways were analyzed for enrichment of differentially expressed proteins. Differentially expressed proteins, which were considered relevant for the cardiovascular system by IPA, were included for further analysis (Data S2). The association of these proteins with cardiovascular disease and cardiac function was suggested by IPA (Data S3). A negative z-score indicates suppression of that pathway, whereas a positive z-score indicates enhancement.

Ultrastructural Analysis of Mitochondria

For ultrastructural analyses, three 8-month-old $\alpha_2^{+/G301R}$ and 3 WT mice were perfusion fixed with 2% glutaraldehyde in 0.1 mol/L cacodylate buffer, pH 7.4, through the left ventricle. Tissue pieces were subsequently postfixed for 1 hour in 1% OsO_4 in 0.1 mol/L cacodylate buffer, stained for 1 hour with 0.5% uranyl acetate in 0.05 mol/L maleate buffer, pH 6.0, dehydrated in graded alcohols, and embedded in Epon (TAAB resin 812; VWR - Bie & Berntsen A/S, Soeborg, Denmark). Ultrathin sections of ≈ 70 nm were obtained with a Leica EM FC6 Cryoultramicrotome, collected on 100 mesh nickel grids and stained with uranyl acetate and lead citrate. Sections were examined using a JEOL JEM-1400+ (JEOL, Freising, Germany) transmission electron microscope.

Histological Analysis of Left Ventricle Tissue

Eight-month-old mice were euthanized, and the left ventricles were dissected in PBS for histological analysis. Left ventricles were fixed in 4% formaldehyde, washed in PBS, embedded in paraffin, and sectioned in 5- μm slices at the level of the papillary muscle. Sections were deparaffinized and processed following standard Masson trichrome staining protocol: 5 minutes in Weigert hematoxylin (1% hematoxylin in 99% ethanol), 5 minutes in picric acid (10 mL saturated picric acid solution in 40 mL 96% ethanol), 10 minutes in

Biebrich scarlet-acid fuchsin solution (300 mg Biebrich scarlet and 100 mg acid fuchsin in 40 mL distilled water and 160 mL 0.2% acetic acid), and 2 minutes in methyl blue solution (1.25 g methyl blue in 100 mL distilled water and 1 mL ethanol). The last 2 steps were followed by 10 minutes in 1% phosphomolybdic acid. Images were taken using Olympus VS120 slide scanner (Olympus, Tokyo, Japan) at $\times 20$ magnification and analyzed using ImageJ software. Measurements were obtained from 31 to 42 cardiomyocytes from each mouse in long-axis and cross-sectional orientation. Measurements of cross-sectional area and longitudinal diameter from each animal were averaged for analysis.

Structure Modeling of the Na,K-ATPase α_2 Isoform

To model the Na,K-ATPase from humans, we used the protein data bank entry 2zxe⁴¹ as a template. The alignments were used to model human Na,K-ATPase α_2 isoform in modeler.⁴² For each template, a total of 100 models were generated. The model identified by the lowest discrete optimized protein energy score⁴³ was used for further analysis.

Statistical Analysis

All data are summarized as the mean value \pm SEM of the sample group. Student *t* test, 1-way ANOVA, or 2-way ANOVA, followed by Bonferroni or Sidak correction for multiple comparisons, was used when appropriate to determine significant differences between means. Differential protein expression in the proteomics data set was analyzed with unpaired *t* test before upload to IPA software for further analysis. A probability (*P*) level of <0.05 was considered significant. In the IPA omics data analysis, *P* values for diseases or function annotations were calculated on the basis of the 1-sided Fisher exact test. Statistical analyses of the functional data were performed with Microsoft Excel or GraphPad Prism software (version 8).

RESULTS

Reduced Expression of the Na,K-ATPase α_2 Isoform in Hearts of $\alpha_2^{+/G301R}$ Mice Was Associated With Increased Expression of the α_1 Isoform But Unchanged Na,Ca-Exchanger Expression

Western blot semiquantification demonstrated an $\approx 25\%$ reduction of the Na,K-ATPase α_2 isoform in the hearts from 3- and 8-month-old $\alpha_2^{+/G301R}$ mice (Figure 1A and 1D). In both age groups of $\alpha_2^{+/G301R}$ mice, this was accompanied by $\approx 25\%$ increased expression of the Na,K-ATPase α_1 isoform (Figure 1B and 1E). No difference in the expression of Na,Ca-exchanger 1 was detected between $\alpha_2^{+/G301R}$ and WT mice in both age groups (Figure 1C and 1F).

Dilation of Ventricles and Impaired Ventricular Function in 8-Month-Old $\alpha_2^{+/G301R}$ Mice

There was no statistical difference in heart rate or respiration frequency between 3- and 8-month-old anaesthetized $\alpha_2^{+/G301R}$ and WT mice (Table S1). Cardiac magnetic resonance imaging (Figure 2A through 2H) showed similar left and right ventricular end-diastolic and end-systolic volumes in 3-month-old WT and $\alpha_2^{+/G301R}$ mice (Figure 2I). Left ventricular ejection fraction (EF; Figure 2J), stroke volume, cardiac output, and cardiac index (Table S1) were similar for 3-month-old mice of both genotypes.

End-diastolic volumes of left and right ventricles as well as end-systolic volume of the left ventricle were increased in 8-month-old $\alpha_2^{+/G301R}$ mice (Figure 2K). Changes in ventricular volume from 3 to 8 months of age were only observed for $\alpha_2^{+/G301R}$ mice. The disarray was associated with decreased left ventricular EF in $\alpha_2^{+/G301R}$ mice (Figure 2L), whereas the difference in right ventricular EF did not achieve statistical significance (Table S1). Stroke volume, cardiac output, and cardiac index were similar between genotypes in 8-month-old mice (Table S1). No difference in left ventricular mass was seen between $\alpha_2^{+/G301R}$ and WT mice in both age groups (Table S1).

The 8-Month-Old $\alpha_2^{+/G301R}$ Mice Showed Reduced Nocturnal Blood Pressure

Both $\alpha_2^{+/G301R}$ and WT mice showed circadian rhythm variations in arterial blood pressure and heart rate that are consistent with murine nocturnal behavior of mice (Figure S2). When compared at the same time of the day, there was no difference in blood pressure and heart rate between 3-month-old $\alpha_2^{+/G301R}$ and WT mice (Figure 3A through 3C). However, 8-month-old $\alpha_2^{+/G301R}$ mice showed a reduction in systolic blood pressure compared with age-matched WT mice (Figure 3D). This reduction was significant at nighttime, when mice are most active. The reduction in nighttime diastolic blood pressure did not achieve significance ($P=0.077$; Figure 3E). No difference in heart rate was observed between 8-month-old mice of the 2 genotypes (Figure 3F).

Cardiomyocytes From 8-Month-Old $\alpha_2^{+/G301R}$ Mice Exhibited Normal Electrophysiological Activity

To assess whether electrophysiological abnormalities may explain reduced ventricular function in 8-month-old $\alpha_2^{+/G301R}$ mice consequent to modified Na⁺ homeostasis, we recorded electrical activity in right atrial trabeculae, posterior part of intercaval region, right atrial wall, and right ventricular wall of isolated hearts. No differences in spontaneous heart rate, resting membrane potential, action potential amplitude, and duration were found between 8-month-old $\alpha_2^{+/G301R}$ and WT mice (Table S2 and Figure

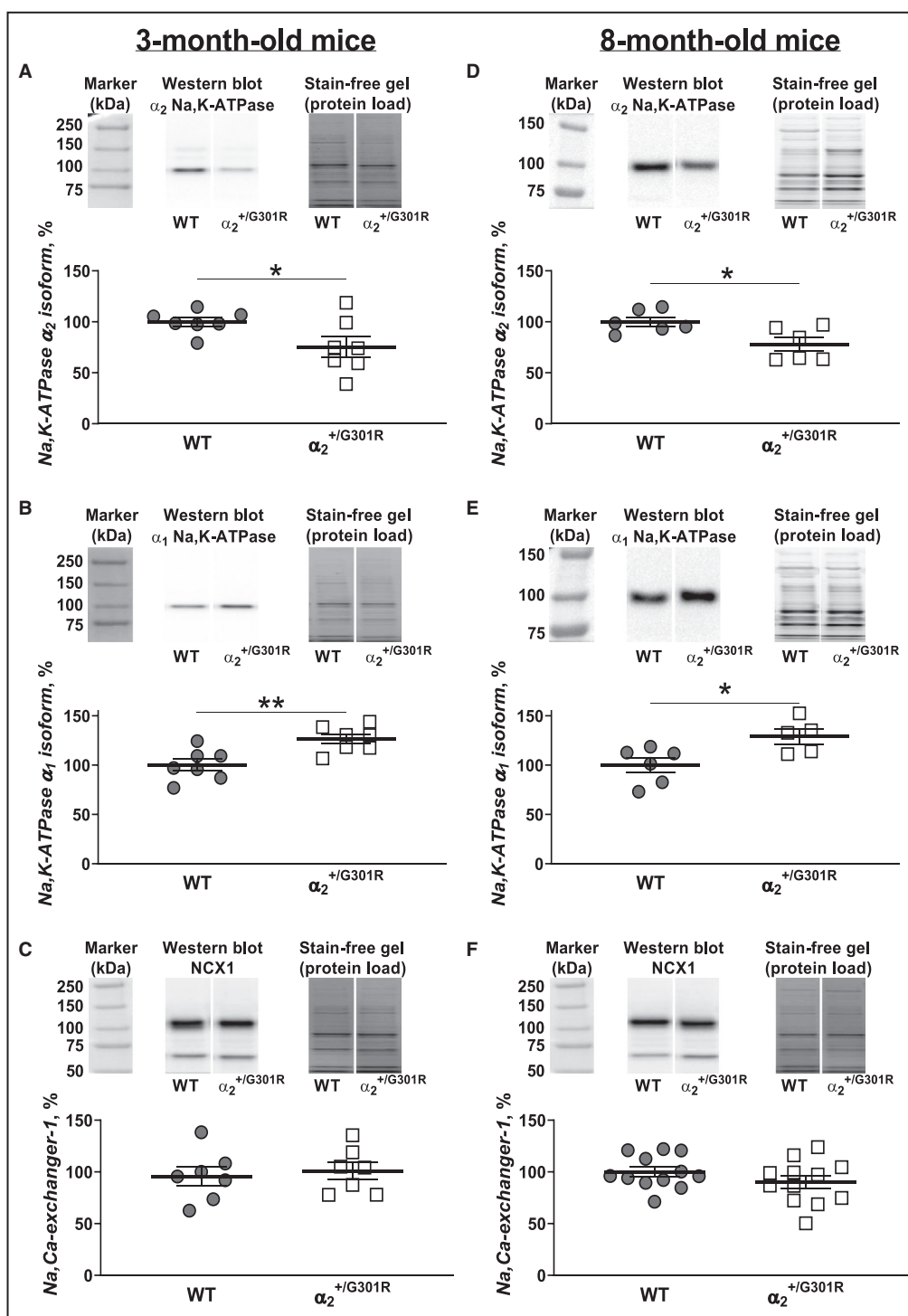


Figure 1. Changed expression of the Na,K-ATPase α isoforms in the heart from $\alpha_2^{+/G301R}$ mice but similar expression of the Na,Ca-exchanger-1.

The hearts from 3- and 8-month-old $\alpha_2^{+/G301R}$ mice showed reduced expression of the Na,K-ATPase α_2 isoform (A, n=7; D, n=6), increased expression of Na,K-ATPase α_1 isoform (B, n=7; E, n=5 to 6), and no change in the expression of Na,Ca-exchanger-1 (NCX1; C, n=7; F, n=12) in comparison with wild type (WT). The expression profile was the same in hearts of 3-month-old (A–C) and 8-month-old (D–F) mice. Upper part of each panel shows representative Western blot bands for the averaged data shown below. The representative bands are shown from the same membrane, as well as the molecular marker shown to the right. The images cropped to include molecular weights from 250 to 50 kDa, as indicated. Total protein load was detected with the stain-free gel, and the corresponding representative bands were cropped to the same molecular weight range. Protein expression was compared using unpaired *t*-test. **P*<0.05 and ***P*<0.01.

S3). This suggests that ion homeostasis and ion transport are not significantly affected in $\alpha_2^{+/G301R}$ cardiomyocytes.

Proton Leak Across the Inner Mitochondrial Membrane and Increased O_2 Consumption in Cardiomyocytes From 8-Month-Old $\alpha_2^{+/G301R}$ Mice

The Na,K-ATPase is a major energy consumer, and its activity affects the cell energetics important for myocardial performance.¹³ To test the impact of the G301R mutation, we assessed the O_2 consumption of the hearts from 3- and 8-month-old $\alpha_2^{+/G301R}$ and WT mice. The residual nonmitochondrial O_2 consumption was increased in hearts from 8-month-old $\alpha_2^{+/G301R}$ mice compared with WT mice (Figure 4A). In 3-month-old mice, nonmitochondrial O_2 consumption was similar between the genotypes (Figure 4A).

There was no difference at state 2 respiration specific to complex I (glutamate and malate) between the groups (Figure 4B and Figure S5). The coupled state 3 respiration with glutamate and malate showed higher O_2 consumption in hearts from 8-month-old $\alpha_2^{+/G301R}$ than in WT mice (Figure 4C). Similarly, maximal coupled state 3 respiration in complex I and II was increased in hearts from 8-month-old $\alpha_2^{+/G301R}$ mice (Figure 4D). The state 4o respiration was also increased in the hearts from 8-month-old $\alpha_2^{+/G301R}$ mice in comparison with WT mice (Figure 4E), suggesting an increased proton leak across the inner mitochondrial membrane.⁴⁴ In contrast, state 3 respiration with glutamate and malate, maximal coupled state 3 respiration in complex I and II, and 4o respiration were similar between genotypes in 3-month-old mice (Figure 4C through 4E).

All experimental groups had similar content of intact mitochondria. The citrate synthase level that serves as marker for mitochondrial content⁴⁵ was similar in both genotypes and age groups (Figure S4). Cytochrome C incubation did not change respiration by >10% in all individual experiments (Figure 4F), except one excluded sample, suggesting intact integrity of the outer mitochondrial membrane.

Hearts From 8-Month-Old $\alpha_2^{+/G301R}$ Mice Showed Increased Oxidative Stress and Increased Lactate Production

We tested oxidative damage in tissue from the left ventricle by measuring malondialdehyde. No difference was detected in the hearts from 3-month-old WT and $\alpha_2^{+/G301R}$ mice, but hearts from 8-month-old $\alpha_2^{+/G301R}$ mice showed elevated malondialdehyde concentrations compared with age-matched WT and 3-month-old $\alpha_2^{+/G301R}$ mice (Figure 5A).

Heart metabolism was assessed in vivo. Magnetic resonance hyperpolarization showed an increased lactate production in hearts from 8-month-old $\alpha_2^{+/G301R}$ mice in comparison with age-matched WT mice (Figure 5B). The levels of alanine and HCO_3^- were similar between the 2 genotypes (Figure 5B). This suggested a shift toward a heart failure-associated metabolism (ie, increased lactate/ HCO_3^- ratio).

$\alpha_2^{+/G301R}$ mice in comparison with age-matched WT mice (Figure 5B). The levels of alanine and HCO_3^- were similar between the 2 genotypes (Figure 5B). This suggested a shift toward a heart failure-associated metabolism (ie, increased lactate/ HCO_3^- ratio).

Increased Capacity of the Src/Ras/Erk1/2 Pathway Downstream From the Na,K-ATPase in Hearts From 8-Month-Old $\alpha_2^{+/G301R}$ Mice

Total expression and phosphorylation levels of protein kinase signaling pathways downstream from the Na,K-ATPase (ie, Src, Erk1/2 kinases, and PLC γ) were assessed in the hearts of 3- and 8-month-old mice. No difference in signaling molecule expression or phosphorylation was detected between 3-month-old $\alpha_2^{+/G301R}$ and WT mice (Figure S6).

The hearts from 8-month-old $\alpha_2^{+/G301R}$ mice had increased expression of total Src kinase but similar level of phosphorylated Src at rest (Figure 6A). Incubation with 1 mmol/L ouabain led to an increased level of phosphorylated Src in the hearts from 8-month-old $\alpha_2^{+/G301R}$ mice compared with WT mice (Figure 6D), suggesting larger capacity for Src phosphorylation in hearts from 8-month-old $\alpha_2^{+/G301R}$ mice (Figure 6F).

Total Erk1/2 expression was increased in hearts from $\alpha_2^{+/G301R}$ mice, but the level of phosphorylated Erk1/2 was decreased at rest (Figure 6B). The difference in the absolute level of phosphorylated Erk1/2 between $\alpha_2^{+/G301R}$ and WT mice did not achieve significance after ouabain incubation (Figure 6E). No difference in total PLC γ or its relative phosphorylation was seen between hearts from 8-month-old $\alpha_2^{+/G301R}$ and WT mice (Figure 6C). The hearts from $\alpha_2^{+/G301R}$ and WT mice incubated with ouabain showed similar phosphorylation levels of PLC γ (data not shown; n=6).

Similar Mitochondrial Membrane Potential in the Hearts From 8-Month-Old Mice of Both Genotypes

We assessed in situ mitochondrial health in the left ventricles from 8-month-old WT and $\alpha_2^{+/G301R}$ mice (Figure 7A). No difference in mitochondrial membrane potential was found between the groups (Figure 7B), suggesting similar mitochondrial polarization. Moreover, as early stages of apoptosis are characterized by mitochondrial disruption, these results suggest that apoptosis state is similar in $\alpha_2^{+/G301R}$ and WT hearts. Disruption of mitochondrial membrane potential with the K^+ ionophore, valinomycin, equally reduced the fluorescence emission from JC-1 aggregates in mitochondrial membrane in WT and $\alpha_2^{+/G301R}$ hearts and was without significant effect on cytosolic JC-1 monomer emission, as expected (Figure 7A). This suggests similar number of mitochondria in both groups.

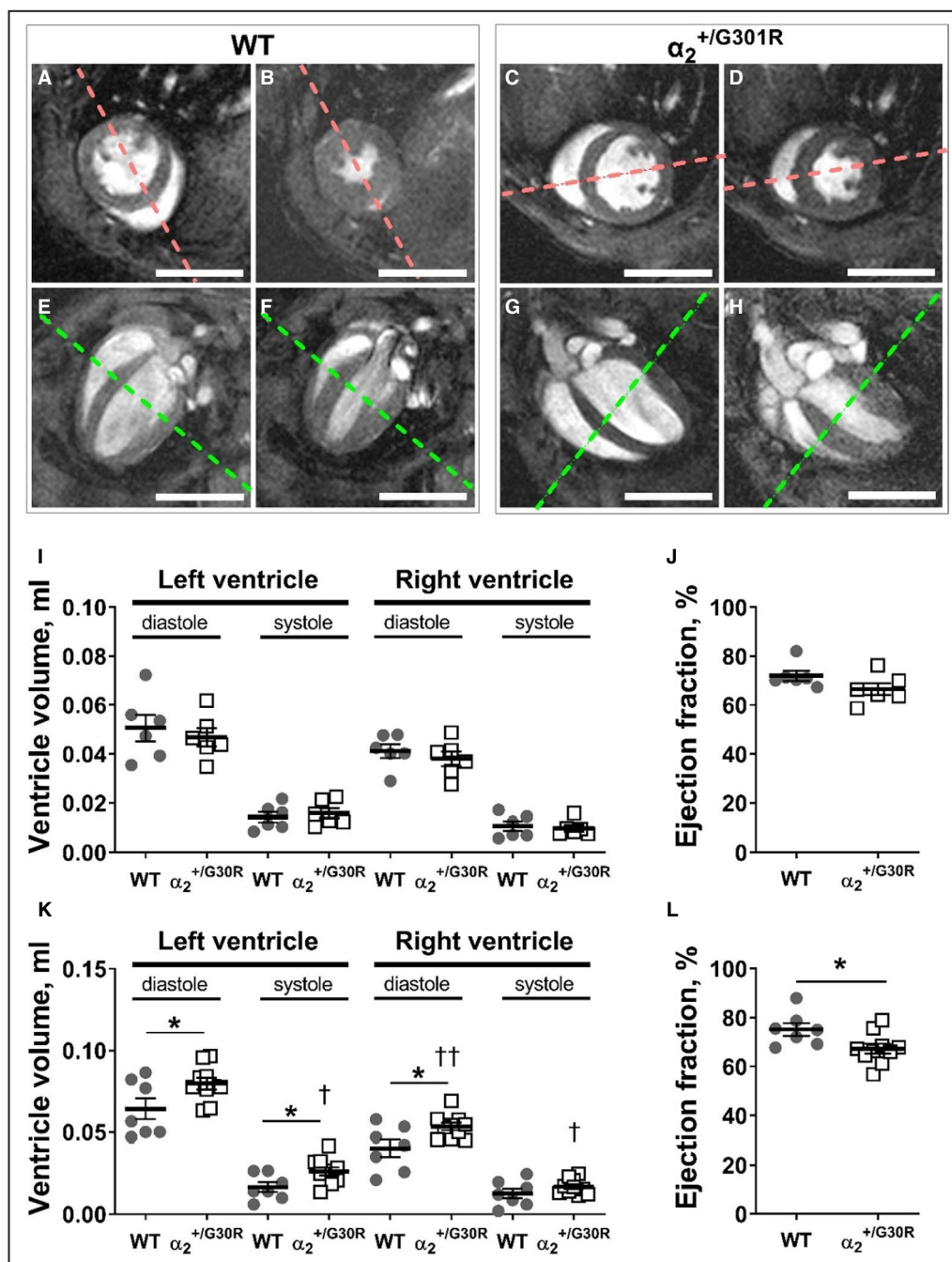


Figure 2. Ventricular dilation and decreased ejection fraction in 8-month-old $\alpha_2^{+/G301R}$ mice.

Representative cardiac magnetic resonance end-diastolic and end-systolic images of the heart from an 8-month-old wild-type (WT) (A and B) and $\alpha_2^{+/G301R}$ mouse (C and D) in the short axis. Representative cardiac magnetic resonance end-diastolic and end-systolic images of the same hearts in the long axis (E–H). The dotted red lines in (A–D) and the dotted green lines (E–H) show the orientation of the long axis and short axis, respectively. Bars (A–H) correspond to 5 mm. Left and right ventricular dimensions and ejection fraction were assessed from short-axis images. No difference in ventricular dimensions (I) and ejection fraction (J) was found between 3-month-old $\alpha_2^{+/G301R}$ (n=6) and WT (n=6) mice. In contrast, both left and right ventricles in 8-month-old $\alpha_2^{+/G301R}$ mice (n=10) were dilated in diastole in comparison with WT mice (K; n=7). Moreover, 8-month-old $\alpha_2^{+/G301R}$ mice also showed increased end-systolic left ventricular volume (K) and reduced ejection fraction (L). The age-related changes in ventricular volume were only observed for $\alpha_2^{+/G301R}$ mice; the end-systolic left and right ventricular volume and end-diastolic right ventricular volume were increased from 3 to 8 months of age. * $P < 0.05$ for comparison of WT and $\alpha_2^{+/G301R}$ mice of the same age group; † $P < 0.05$ and †† $P < 0.01$ for comparison of mice of the same genotype at 3 and 8 months of age (2-way ANOVA with Sidak multiple comparisons test).

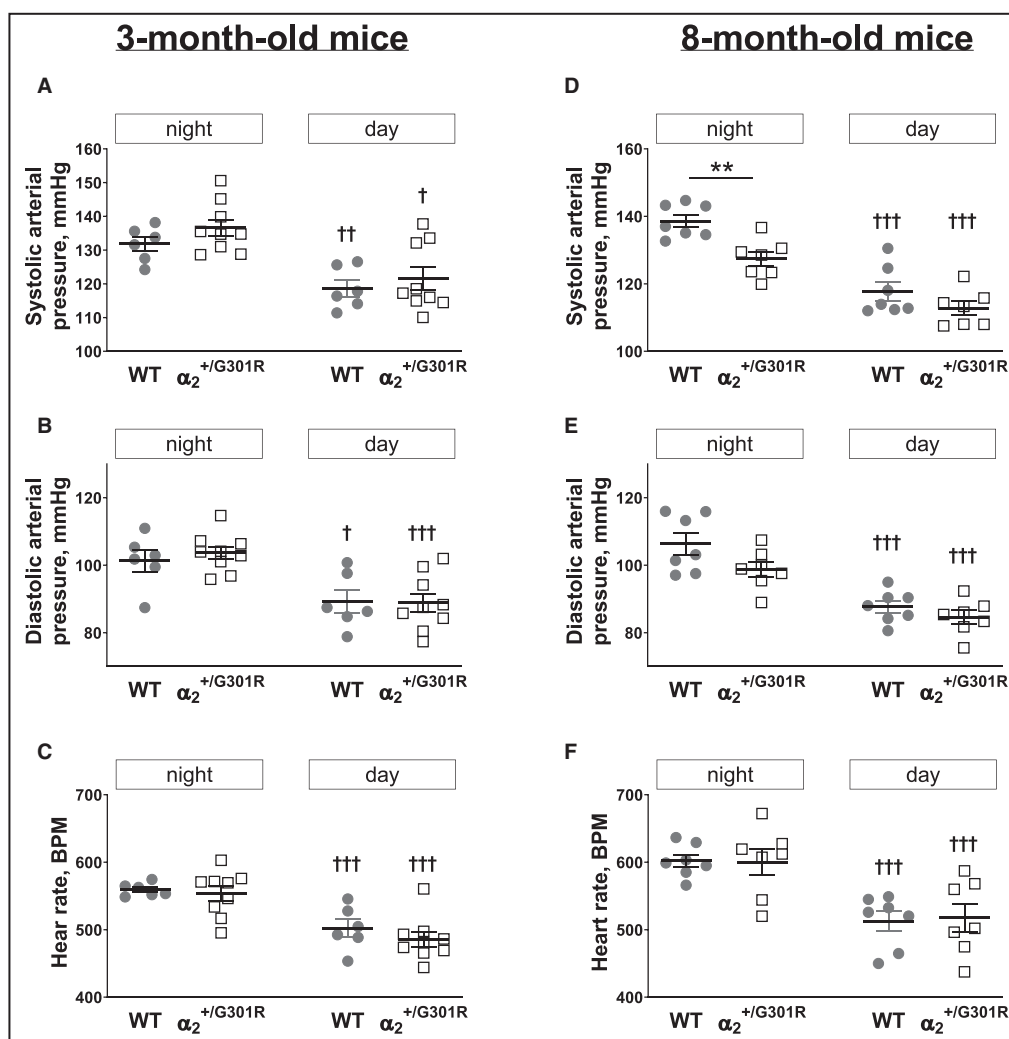


Figure 3. The 8-month-old $\alpha_2^{+/G301R}$ mice showed lower nocturnal blood pressure than wild-type (WT) mice.

Averaged systolic (A and D) and diastolic (B and E) blood pressure and heart rate (C and F) of 3-month-old (A–C; n=6–9) and 8-month-old (D–F; n=7) $\alpha_2^{+/G301R}$ and WT mice. Blood pressure and heart rate were averaged over the period where night activity of mice was most prominent (from 8 PM to 10 PM) and the day activity was minimal (from 12 AM to 2 PM). For circadian variations, see also Figure S2. BPM indicates beats per minute. ** $P < 0.01$ for comparison between WT and $\alpha_2^{+/G301R}$ mice of the same age; † $P < 0.05$, †† $P < 0.01$, and ††† $P < 0.001$ for comparison of mice of the same genotype at day and night (2-way ANOVA with Sidak multiple comparisons test).

Similar Mitochondrial Ultrastructure and Cardiomyocyte Morphology in Both Genotypes

Mitochondrial ultrastructure was assessed in cross-sections of left ventricle tissue from 8-month-old mice using transmission electron microscopy. Similar mitochondrial ultrastructure was observed in both genotypes (Figure 7C). Cardiac tissue morphology was assessed in left ventricle cross-sections stained with Masson trichrome. There was no difference between genotypes in cross-sectional area of cardiomyocytes from 8-month-old mice (Figure S7A and S7B). Also, cardiomyocyte diameter

measured in the long axis was similar in both genotypes (Figure S7C and S7D). No infarctions were detected in any of the mice of both genotypes.

Proteomics Data Analysis Suggested the Molecular Basis for the Cardiac Phenotype in 8-Month-Old $\alpha_2^{+/G301R}$ Mice

Our proteomic data provided assessment of relative protein expression changes. Data are available via ProteomeXchange with identifier PXD028952. We identified 2888 mapped proteins, thereof 181 significantly up-regulated and 22 down-regulated analysis-ready proteins

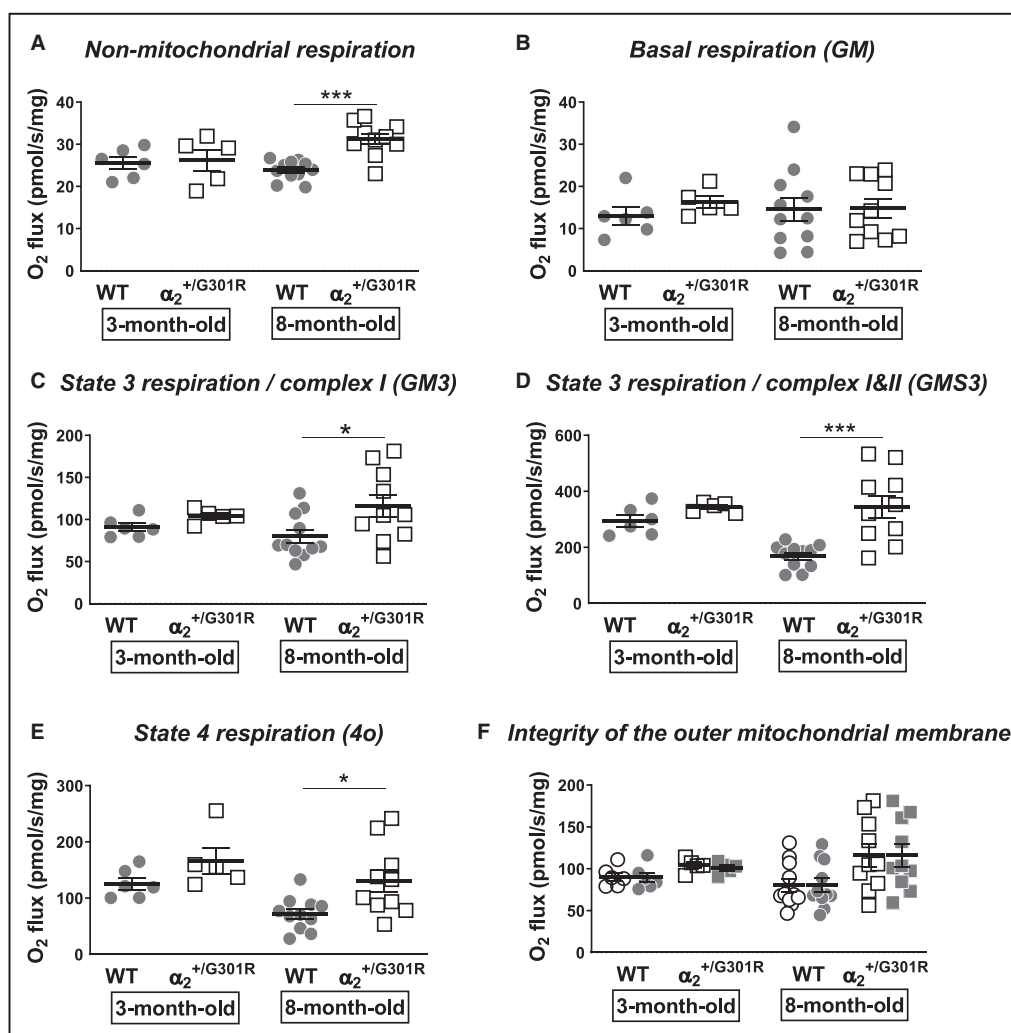


Figure 4. The hearts from 8-month-old $\alpha_2^{+/G301R}$ mice showed mitochondrial uncoupling.

Left ventricles from 3-month-old ($n=5-6$) and 8-month-old ($n=10-11$) $\alpha_2^{+/G301R}$ and wild-type (WT) mice were compared for the following parameters: uncoupled, nonmitochondrial respiration (A), basal respiration (GM) (B), state 3 respiration in complex I (GM3) (C), state 3 respiration in complex I and II (GMS3) (D), state 4 respiration (4o) (E), and the outer mitochondrial membrane integrity (F), where open labels show O_2 consumption before and filled labels after cytochrome C incubation. Genotypes in each age group were compared using unpaired t test. * $P<0.05$ and *** $P<0.001$. See also representative traces in Figure S5. GM indicates glutamate and malate; and GM3, state 3 respiration with glutamate and malate.

in the hearts from $\alpha_2^{+/G301R}$ mice in comparison with WT mice (Data S1). A total of 145 of the proteins were associated with the cardiovascular system (Data S2). We identified several cardiovascular conditions that were correlated with the expressional pattern in the hearts from $\alpha_2^{+/G301R}$ mice. These were primarily conditions associated with systolic dysfunction (Data S3).

The reduced ejection fraction was associated with downregulation of several components of the troponin-tropomyosin complex and cardiac α -actin (Figure S8A). Together with the finding of upregulation of myosin light chain 7 and α -actinin 2, these data suggested a reduced Ca^{2+} sensitivity of the contractile machinery in $\alpha_2^{+/G301R}$ cardiomyocytes (Figure S8A). No difference in the expression

of Ca^{2+} transporting proteins was found between the hearts from $\alpha_2^{+/G301R}$ and WT mice (Figure S8B).

The proteomics data analysis confirmed that the expression of the Na,K-ATPase α_1 isoform was increased, whereas the α_2 isoform was decreased, in the hearts from $\alpha_2^{+/G301R}$ mice (Figure S9A). On the basis of upregulation of protein phosphatases, mitogen-activated protein kinase kinase 3, and Ras family proteins, the analysis suggested increased Src/Ras/Erk1/2 signaling in hearts from 8-month-old $\alpha_2^{+/G301R}$ mice (Figure S9B and S9C). Increased oxidative stress in the hearts from $\alpha_2^{+/G301R}$ mice was predicted on the basis of upregulation of enzymes involved in generation of ROS and regulation of the cellular oxidation-reduction state (Figure S10).

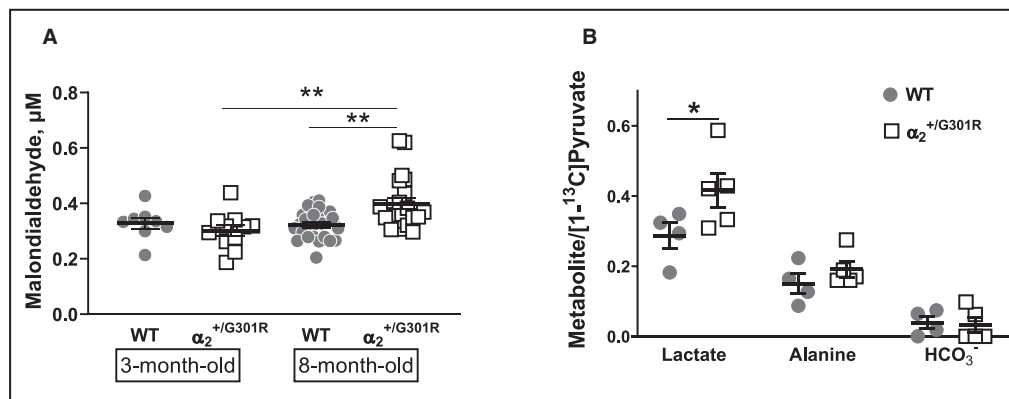


Figure 5. Increased lipid peroxidation and lactate production in the hearts from 8-month-old $\alpha_2^{+/G301R}$ mice.

A, Lipid peroxidation was assessed as a concentration of malondialdehyde in the left ventricle. No difference in malondialdehyde concentration was seen between genotypes of 3-month-old mice ($n=8-11$), but hearts from 8-month-old $\alpha_2^{+/G301R}$ mice ($n=21$) showed elevated malondialdehyde concentrations in comparison with both hearts from age-matched wild-type (WT) mice ($n=26$) and 3-month-old $\alpha_2^{+/G301R}$ mice. **B**, Magnetic resonance hyperpolarization showed an increased pyruvate conversion ratio to lactate in the hearts from 8-month-old $\alpha_2^{+/G301R}$ mice ($n=5$) in comparison with age-matched WT mice ($n=4$). No difference in conversion ratio to alanine and bicarbonate was seen. Malondialdehyde concentrations in the groups and at different ages were compared using 2-way ANOVA with Sidak multiple comparisons test. The level of pyruvate metabolite products was compared between the groups using unpaired *t*-test. * $P<0.05$ and ** $P<0.01$.

DISCUSSION

This study addressed the importance of migraine-associated mutation of the Na,K-ATPase α_2 isoform for cardiovascular function. In a mouse model for FHM2, we found that hearts from 8-month-old $\alpha_2^{+/G301R}$ mice exhibited dilation of left and right ventricles and reduced left ventricular EF but no left ventricular hypertrophy. The cardiac phenotype in 8-month-old $\alpha_2^{+/G301R}$ mice was associated with proton leak across the inner mitochondrial membrane, increased oxidative stress, and a heart failure-associated metabolic shift toward glycolysis accompanied by increased lactic acid production. Our data indicated that imbalanced Na,K-ATPase-dependent Src/Ras/Erk1/2 signaling underlies mitochondrial dysfunction, leading to increased generation of ROS in 8-month-old $\alpha_2^{+/G301R}$ mice. Our finding of a link between FHM2-associated mutation and cardiac dysfunction provides novel insight into the association between migraine and cardiovascular disease.

Oxidative Stress and Suppressed Cardiac Function in $\alpha_2^{+/G301R}$ Mice Were Associated With Altered Cardiac Metabolism

The hemodynamically or metabolically stressed heart often returns to a pattern of fetal metabolism, where it depends primarily on glucose and lactate for energy.⁴⁶ This cardiac metabolic shift toward glycolysis is known as fetal programming and is a well-known feature in

the failing heart and in cardiomyopathy.⁴⁷ We suggest that fetal programming in hearts from 8-month-old $\alpha_2^{+/G301R}$ mice is a consequence of chronically increased oxidative stress over many months. In support of this suggestion, our data demonstrated a similar production of HCO₃⁻ in $\alpha_2^{+/G301R}$ and WT mice. This may reflect that during the experiment, O₂ availability was sufficient to maintain pyruvate dehydrogenase flux. Maintained pyruvate dehydrogenase flux, increased glycolysis, and increased production of lactic acid in $\alpha_2^{+/G301R}$ mice suggest a metabolic shift toward fetal programming.

Cardiac fetal programming is closely associated with increased generation of ROS.⁴⁷ ROS are produced continually in mitochondria as a by-product of normal respiration through the one-electron reduction of molecular oxygen.⁴⁸ We found a markedly increased O₂ consumption in the hearts from 8-month-old $\alpha_2^{+/G301R}$ mice. Our results indicated that this is attributable to increased proton leak across the inner mitochondrial membrane and increased O₂ consumption by nonmitochondrial oxidation processes. Chronic heart failure was previously reported to reduce mitochondrial membrane potential,⁴⁹ and this was suggested to contribute to cardiac remodeling.⁵⁰ We demonstrated that mitochondria in hearts from 8-month-old $\alpha_2^{+/G301R}$ mice were able to maintain a hyperpolarized mitochondrial membrane potential similar to WT mice. Also, mitochondrial ultrastructure was similar between the 2 genotypes. Both citrate synthase assay and JC-1 data suggested similar number of mitochondria. The dissociation between mitochondrial

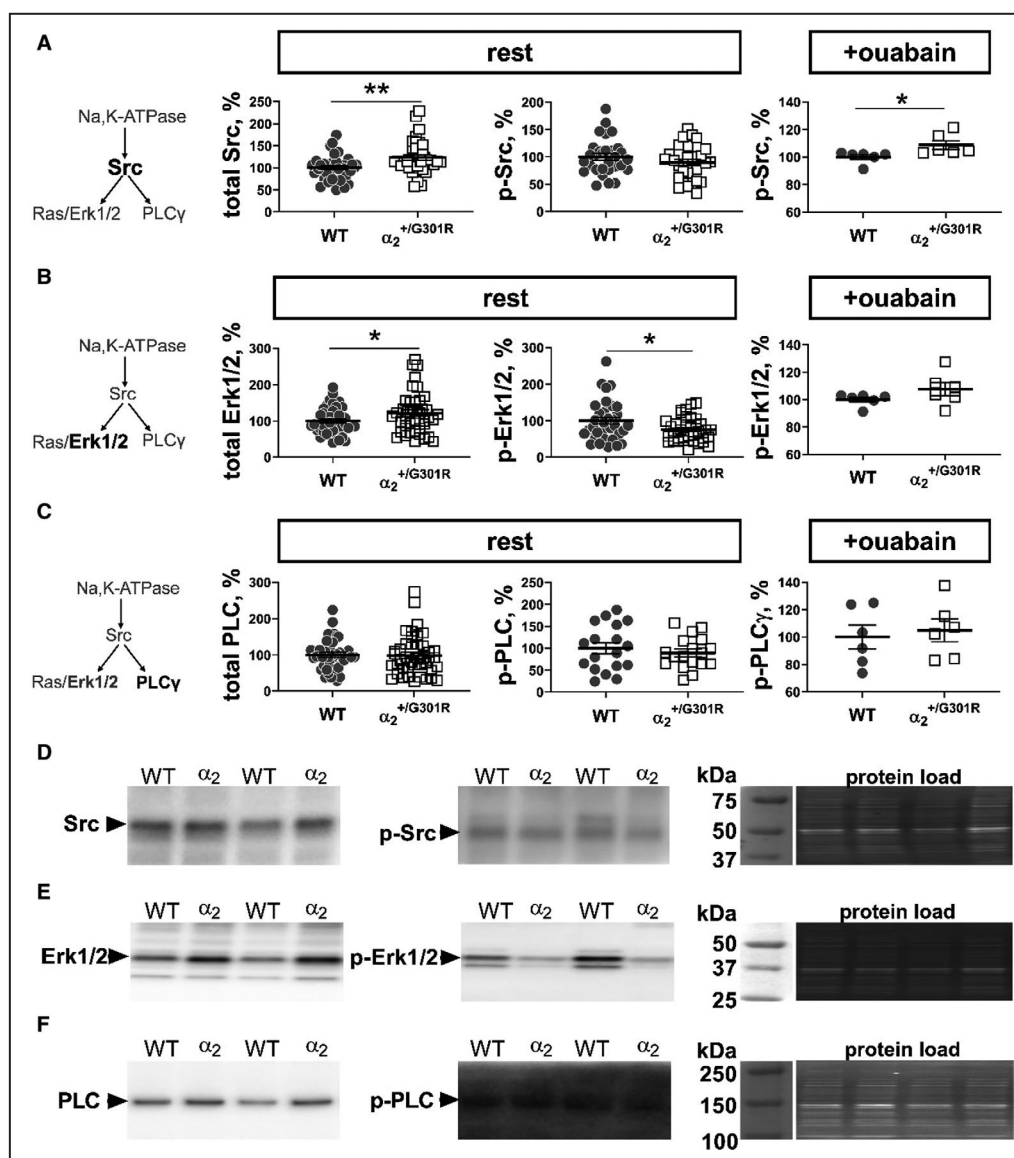


Figure 6. The hearts from 8-month-old $\alpha_2^{+/G301R}$ mice showed modified signaling of pathways downstream from the Na,K-ATPase.

A semiquantification of expressional changes of total Src kinase (n=36) and the level of Src phosphorylation at Tyr418 (**A**; n=30); total Erk1/2 kinase (n=42) and its Thr202/Tyr204 phosphorylation level (**B**; n=36); and total PLCγ (n=42) and the level of its Tyr783 phosphorylation (**C**; n=18). When the hearts were incubated for 30 minutes with 1 mmol/L ouabain, the level of phosphorylated Src was significantly increased (**A**; n=6). The phosphorylation level of Erk1/2 after 1 mmol/L ouabain incubation tended to increase in $\alpha_2^{+/G301R}$ hearts in comparison with wild-type (WT) mice, but this did not achieve significance (**B**; n=6; $P=0.17$). Representative images for Src (**D**), Erk1/2 (**E**), and PLCγ (**F**) semiquantification Western blot experiments that are averaged (**A–C**), respectively. Left images correspond to total protein of interest (Src, Erk1/2, and PLCγ, respectively). Images in the center correspond to phosphorylated protein of interest (p-Src, p-Erk1/2, and p-PLCγ, respectively), as indicated. Molecular weight markers and total protein load in the membrane detected with stain-free gels are shown to the right. All representative images were cropped to the size identified by molecular marker (**D–F**), respectively. All images are cropped to include at 3 molecular weight markers positioned both above and below the band. Before incubation with the antibodies, the membrane was divided into 2 parts: the upper part, above 75 kDa, was used to detect PLCγ and p-PLCγ; and the lower part, below 75 kDa, was used to detect either Src and p-Src or Erk1/2 and p-Erk1/2, respectively. The expression was normalized to total protein load for the corresponding probe. An average level for the WT group was taken as 100%. Protein expression was compared between genotypes using unpaired *t*-test. * $P<0.05$ and ** $P<0.01$.

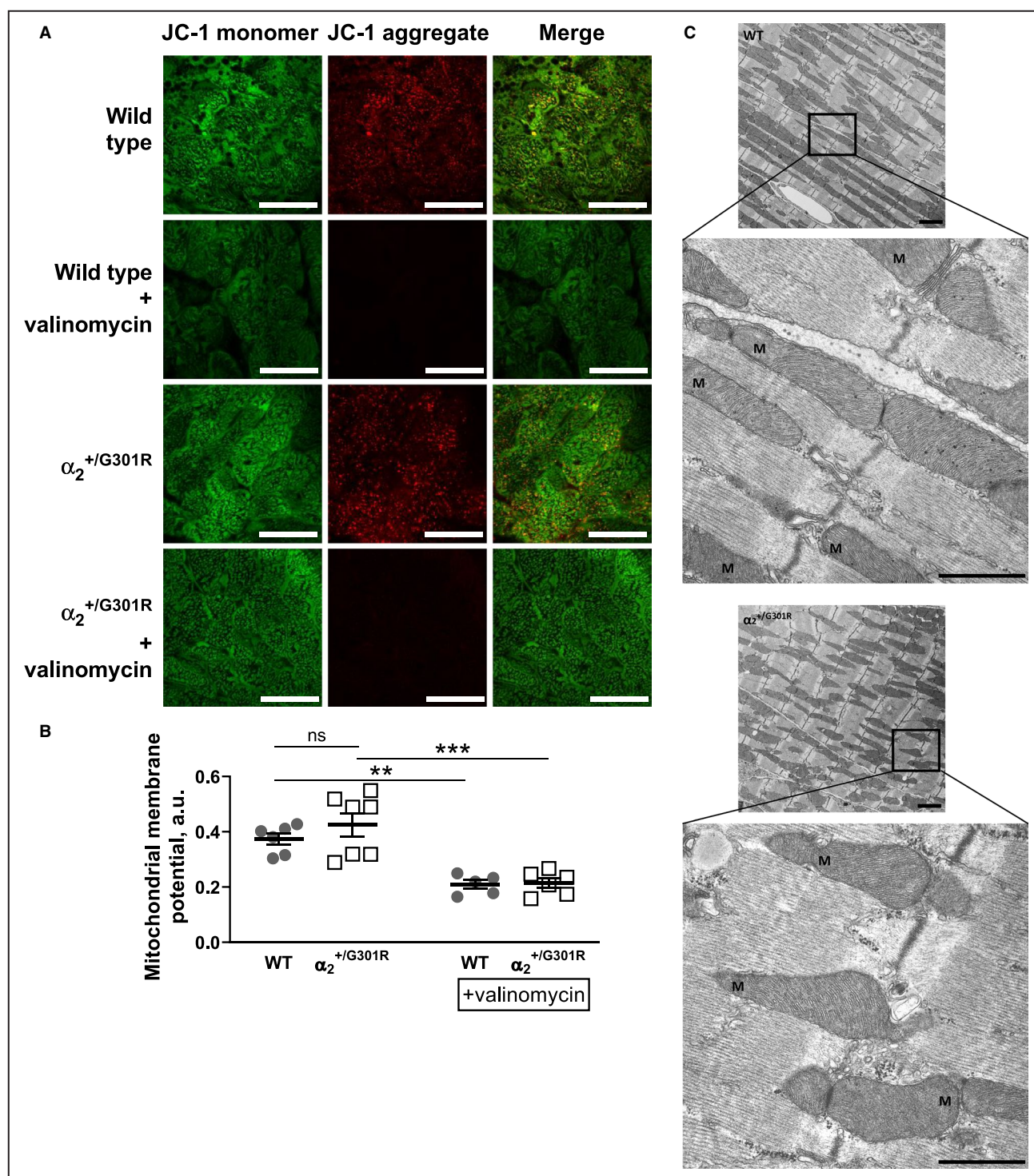


Figure 7. No difference in mitochondrial health between the hearts from 8-month-old wild-type (WT) and $\alpha_2^{+/G301R}$ mice.

Fresh cross-sectional myocardial slices were loaded with the fluorescent dye, 5,5',6,6'-tetrachloro-1,1',3,3'-tetraethylbenzimidazolo carbocyanine iodide (JC-1). When JC-1 is in its monomeric cytoplasmic form, it emits green light; and in its aggregated form, which accumulates in mitochondria (M) in a potential-dependent manner, it emits red light (**A**). The fluorescence ratio (red/green) reflects mitochondrial membrane potentials in the hearts from WT (n=6) and $\alpha_2^{+/G301R}$ mice (**B**; n=7). To test the signal specificity, some slices were pretreated with valinomycin, a potassium ionophore and an uncoupler of mitochondrial respiration that causes collapse of the mitochondrial membrane potential (WT, n=5; and $\alpha_2^{+/G301R}$, n=6). Bars in **A** correspond to 50 μ m. Fluorescence ratio in the 2 genotypes as well as the fluorescence ratio before and after valinomycin in each group were compared using 2-way ANOVA with Sidak multiple comparisons test. ** $P < 0.01$ and *** $P < 0.001$. Morphological analysis of mitochondria (WT, n=3; and $\alpha_2^{+/G301R}$, n=3) were performed by transmission electron microscopy (**C**). Scale bars on high-magnification micrographs: 1 μ m; and on low-magnification micrographs: 2 μ m. Ns indicates no significant difference.

membrane potential generation and its use of oxygen for mitochondria-dependent ATP synthesis indicates mitochondrial uncoupling in the hearts of 8-month-old $\alpha_2^{+/G301R}$ mice. Oxidative stress facilitates opening of permeability transition pores in the mitochondrial membrane, which on opening induce proton leak across the inner mitochondrial membrane,^{51,52} as observed in 8-month-old $\alpha_2^{+/G301R}$ mice. This proton leak further increases oxidative stress. Thus, a positive feedback loop is established. In agreement with this finding, it has previously been demonstrated that the Na,K-ATPase plays a central role in this oxidative stress-dependent positive feedback loop.^{53,54} Moreover, the Na,K-ATPase is suggested to contribute to oxidation-reduction-dependent β -adrenergic signaling²⁰ (ie, we expect oxidative stress to increase during increased nocturnal activity, and we expect this increase to be larger in $\alpha_2^{+/G301R}$ mice). To summarize, we suggest that increased level of oxidative stress in the hearts from $\alpha_2^{+/G301R}$ mice originates from the metabolic shift as well as mitochondrial uncoupling (Figure 8).

In heart failure, ROS are suggested to modify myofibrillar proteins, including cardiac α -actin and tropomyosin, by oxidation, resulting in changed structure and function of the contractile machinery.^{55,56} This is associated with release of troponin from the myocardium to the bloodstream, both in acute and chronic heart failure.⁵⁷ In the present study, 8-month-old $\alpha_2^{+/G301R}$ mice that exhibited reduced EF and ventricular dilation showed reduced levels of cardiac α -actin and components of the troponin-tropomyosin complex in the cardiac tissue. We suggest that these changes leading to reduced Ca^{2+} sensitivity in the contractile machinery form the basis of systolic dysfunction in 8-month-old $\alpha_2^{+/G301R}$ mice and that they are caused by oxidative damage. Interestingly, this is not the first time an association between systolic dysfunction and changed expression of the Na,K-ATPase has been observed. In humans, the concentration of the Na,K-ATPase was shown to be reduced in the early stages of heart failure⁷ and in dilated cardiomyopathy.⁸ Although the causal relation was not addressed, the changed expression of Na,K-ATPase in those studies is likely secondary to cardiac pathology. In contrast, we herein demonstrated that inherited changes in the expression of Na,K-ATPase can cause cardiovascular disease.

Blood Pressure Changes in 8-Month-Old $\alpha_2^{+/G301R}$ Mice May Be a Result of Reduced Cardiac Function

We have previously reported unchanged ex vivo vascular tone of small peripheral arteries from $\alpha_2^{+/G301R}$ mice, suggesting unchanged total peripheral resistance.²⁷ In the present study, 8-month-old $\alpha_2^{+/G301R}$ mice showed reduced nocturnal blood pressure.

There may be several reasons for this inconsistency. Although cardiac output was similar in anaesthetized 8-month-old $\alpha_2^{+/G301R}$ and WT mice, reduced ability to increase cardiac output on physical activity in $\alpha_2^{+/G301R}$ may be responsible for reduced blood pressure. Consistent with this possibility, the difference in blood pressure between genotypes was observed only at night when mice are active. However, other explanations, such as reduced sympathetic tone in 8-month-old $\alpha_2^{+/G301R}$ mice, cannot be excluded and require further investigation. Nevertheless, the observed reduction in arterial blood pressure is highly unlikely to cause the cardiac phenotype in 8-month-old $\alpha_2^{+/G301R}$ mice.

Our findings in 3-month-old mice are in line with other reports on unchanged blood pressure on cardiac- and vascular smooth muscle cell-specific knockout of the Na,K-ATPase α_2 isoform in mice.⁵⁸ More important, these measurements were done with tail-cuff method (ie, in stressed mice). Another telemetry study reported elevated blood pressure in mice with smooth muscle-specific knockout of the Na,K-ATPase α_2 isoform, suggesting elevated total peripheral resistance.⁵⁹ This is in contrast to our findings and may be a result of tissue-specific knockout generation. To our knowledge, no study on aged mice with the Na,K-ATPase expression manipulation is available yet.

Changed Expression of the Na,K-ATPase α Isoforms in the Heart of $\alpha_2^{+/G301R}$ Mice Did Not Appear to Affect Electrical Activity of Cardiomyocytes

Previous expression analyses of the $\alpha_2^{+/G301R}$ mice showed a decrease in expression of the Na,K-ATPase α_2 isoform in brain lysate²⁵ and in the arterial wall.²⁷ In the present study, we also found reduced expression of the α_2 isoform accompanied by increased expression of the α_1 isoform in the hearts from $\alpha_2^{+/G301R}$ mice compared with WT mice. The increased α_1 expression may be compensatory for the lack of electrogenic activity of the α_2 isoform.^{4,10} In fact, similar membrane potentials in cardiomyocytes from the 2 genotypes were seen, and 3-month-old mice of both genotypes showed similar EF. However, increase of the cardiac α_1 isoform was observed in both 3- and 8-month-old $\alpha_2^{+/G301R}$ mice, suggesting that this cannot directly explain the decline in cardiac performance in 8-month-old $\alpha_2^{+/G301R}$ mice. Therefore, it is unlikely that the observed cardiac functional abnormalities are a result of changed ion transport.

It has previously been reported that heterozygous knockout of either α_1 or α_2 isoform of the Na,K-ATPase affected the nontargeted α isoform

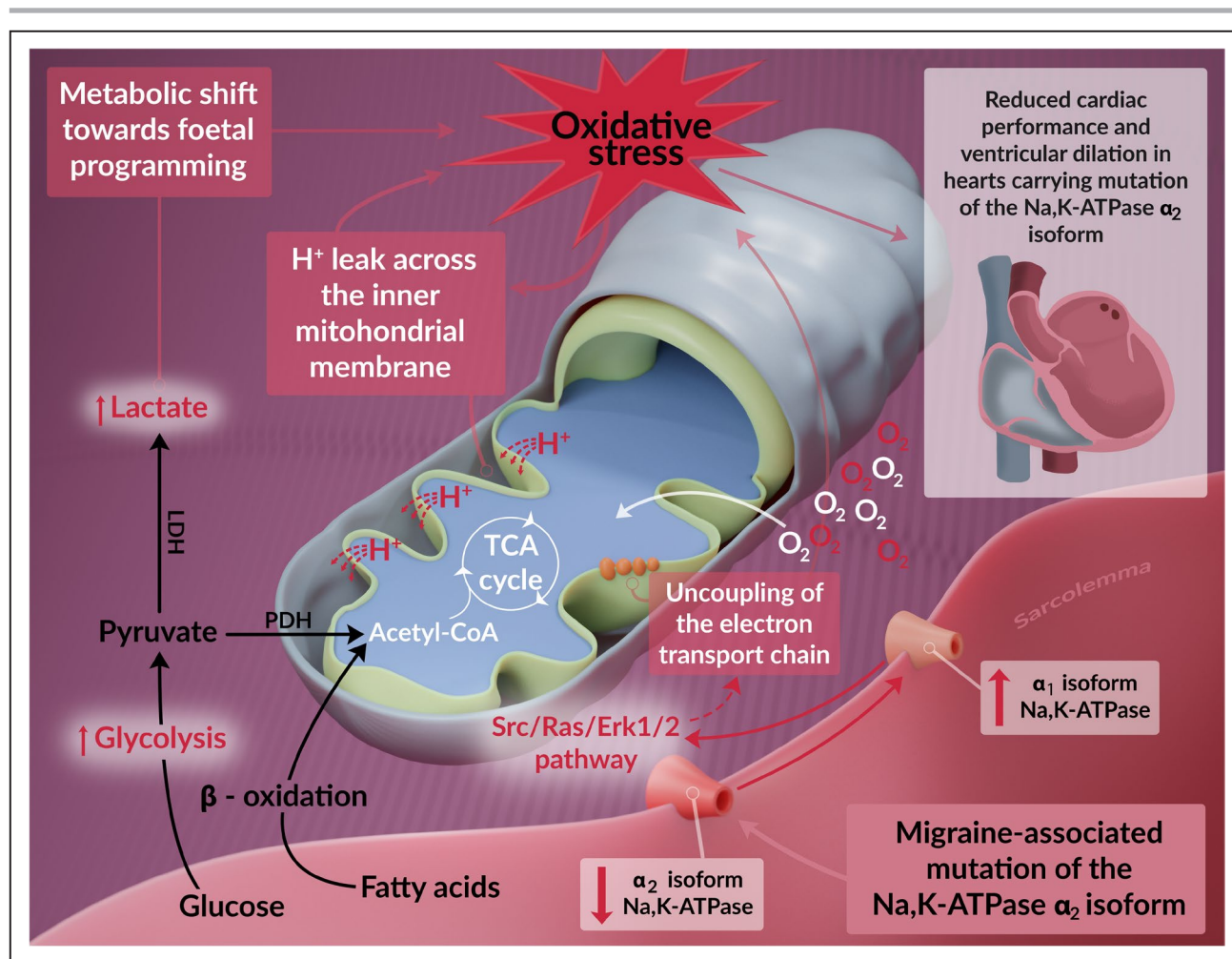


Figure 8. Summary of metabolic changes in the heart with mutation of the Na,K-ATPase α_2 isoform.

Migraine-associated mutation led to reduced expression of the Na,K-ATPase α_2 isoform that, in turn, increased the expression of the α_1 isoform. This was associated with unbalanced signaling of the Src/Ras/Erk1/2 pathway, leading to uncoupling of the electron transport chain. Mitochondrial uncoupling in combination with heart failure-associated metabolic shift toward fetal programming accompanied by increased level of lactic acid and H^+ leak through the inner mitochondrial membrane led to oxidative stress. Oxidative stress further increases H^+ leak across the inner mitochondrial membrane and thus establishes a positive feedback loop. This was associated with ventricular dilation and reduced cardiac performance. Pathological conditions are identified in red font, red arrows, and red text boxes. LDH indicates lactate dehydrogenase; PDH, pyruvate dehydrogenase; and TCA, tricarboxylic acid.

differently. The α_2 isoform was increased in hearts from $\alpha_1^{+/-}$ mice, whereas the α_1 isoform expression was unchanged in hearts from $\alpha_2^{+/-}$ mice.⁶⁰ On this background, the current finding of α_1 isoform up-regulation in hearts from $\alpha_2^{+/G301R}$ mice is surprising. The expression of the Na,Ca-exchanger and several other Ca^{2+} transporting proteins was similar in hearts from WT and $\alpha_2^{+/G301R}$ mice. Similar expression in both genotypes of the Na,Ca-exchanger is in contrast to previous reports on reciprocal regulation of the expression of the Na,K-ATPase α_2 isoform and the Na,Ca-exchanger,^{61,62} suggesting, at least at the expression level, that Na^+ and Ca^{2+} exchange is not affected in $\alpha_2^{+/G301R}$ mice.

Changed Signaling of the Src/Ras/Erk1/2 Pathway Was Associated With Mitochondrial Uncoupling in $\alpha_2^{+/G301R}$ Mice

The cardiac Na,K-ATPase is suggested to have a distinct function in oxidative stress amplification.^{20,54} Thus, binding of cardiotonic steroids to the Na,K-ATPase or its chemical modification by intracellular signaling activates Src kinase that, in turn, transactivates the epidermal growth factor receptor, which initiates Ras/Erk1/2 signaling.¹⁶ This Src/Ras/Erk1/2 pathway in cardiomyocytes is suggested to increase generation of ROS, which is prevented by additive inhibition of mitochondrial complexes I and III.¹⁶ The 8-month-old $\alpha_2^{+/G301R}$ mice showed increased signaling

capacity of the Src/Ras/Erk1/2 cascade and amplification of this signaling after inhibition of the Na,K-ATPase by ouabain. This larger capacity for activation suggests that under hemodynamic or metabolic stress, the hearts from 8-month-old $\alpha_2^{+/G301R}$ mice may experience increased activation of the Src/Ras/Erk1/2 pathway. Accordingly, proteomics data analysis predicted increased Src/Ras/Erk1/2 signaling in 8-month-old $\alpha_2^{+/G301R}$ mice. The increased total Src expression may be compensatory to the increased expression of the Na,K-ATPase α_1 isoform, which is suggested to regulate the phosphorylation level of Src,⁶³ and thus, keeping the level of activated Src within a normal range under resting conditions. This produces, however, a background for misbalance in the maximal activation capacity leading to disproportional Src/Ras/Erk1/2 signaling on Src activation.

The Na,K-ATPase-dependent ROS pathway is suggested to be potentiated on carbonylation of the α_1 isoform directly by ROS.⁵³ Moreover, in heart failure, ROS were shown to reversibly inhibit the Na,K-ATPase through oxidative modification involving NADPH oxidase and glutathionylation.⁶⁴ Notably, an upregulation in enzymes implicated in generation of ROS and regulation of cellular oxidation-reduction state was detected in hearts from 8-month-old $\alpha_2^{+/G301R}$ mice. Thus, oxidative stress, increasing with age, might be amplified by the increased expression of the Na,K-ATPase α_1 isoform in the hearts from $\alpha_2^{+/G301R}$ mice. Therefore, α_1 Na,K-ATPase-ROS amplification through the Src/Ras/Erk1/2 pathway may be responsible for mitochondrial uncoupling and thereby attributable to ROS generation.⁵⁴ Of note, the hearts from 3-month-old $\alpha_2^{+/G301R}$ and WT mice showed similar capacity and signaling of the Src/Ras/Erk1/2 pathway, which was associated with similar mitochondrial function and normal levels of oxidative stress in both genotypes. In contrast to the Src/Ras/Erk1/2 signaling pathway, we found no changes in PLC γ /inositol trisphosphate-receptor signaling, which previously has been proposed to be associated with the Na,K-ATPase.^{14,17} This is in line with the functional data suggesting similar Ca²⁺ homeostasis in cardiomyocytes from mice of both genotypes.

This study has some limitations to be considered. First, the G301R mutation, that we have studied, is known to cause a severe FHM2 phenotype.²⁶ However, this is 1 of >100 mutations in the *ATP1A2* gene that are known to be associated with FHM2. These *ATP1A2* mutations have been suggested to have different consequences for the α_2 isoform expression and membrane localization.⁶⁵ Whether other *ATP1A2* mutations also affect cardiac function remains to be studied. Second, the use of a mouse model to study the association between FHM2 and cardiovascular disease has inherent limitations in representing human beings. Thus, it remains to be investigated whether patients with FHM2 exhibit similar expression changes of Na,K-ATPase α isoforms and

a cardiac phenotype similar to what we observed in $\alpha_2^{+/G301R}$ mice. Finally, cardiac output, measured by magnetic resonance imaging, was assessed in anesthetized mice, which might affect the cardiovascular system. Direct radiotelemetric measurement of cardiac output would have been preferable, but this is not yet technically feasible.

In conclusion, our results suggest that the FHM2-associated G301R mutation of the Na,K-ATPase α_2 isoform leads to cardiac dysfunction and ventricular dilation accompanied by metabolic shift in cardiomyocytes. We provided functional evidence that this relates to mitochondrial uncoupling that was associated with oxidative stress. We suggest that these abnormalities are mediated via amplified Na,K-ATPase-dependent ROS signaling through the Src/Ras/Erk1/2 pathway. These findings propose a novel mechanistic background for comorbidity between migraine and cardiovascular disease.⁶⁶⁻⁸⁴

ARTICLE INFORMATION

Received March 27, 2021; accepted December 21, 2021.

Affiliations

Department of Biomedicine, Health (C.S., R.N., K.L.-H., M.N., C.A., V.M.), MR Research Centre, Department of Clinical Medicine (S.R., C.L.) and Department of Clinical Medicine (J.J., K.L.-H., N.R.J., H.E.B.), Aarhus University, Aarhus, Denmark; Department of Chemistry and Bioscience (P.D.R.) and Department of Health Science and Technology (M.N.), Aalborg University, Aalborg, Denmark; Department of Cardiology, Viborg Regional Hospital, Viborg, Denmark (N.T.K.); Department for Clinical Biochemistry and Pharmacology, Odense University Hospital, Odense, Denmark (H.C.B.); Department of Biotechnology and Biomedicine, Technical University of Denmark, Kgs. Lyngby, Denmark (J.P.M.); Department of Clinical Genetics, Aarhus University Hospital, Aarhus, Denmark (K.L.); Department of Human and Animal Physiology, Biological Faculty, Lomonosov Moscow State University, Moscow, Russia (D.A.); and Department of Biomedical Sciences, Copenhagen University, Copenhagen, Denmark (C.A.).

Acknowledgments

We thank Casper Carlsen Elkjær (Aarhus University Hospital) for technical assistance with respirometry experiments and citrate synthase activity assay. We thank Jane Holbæk Roenn and Viola Smed Mose Larsen (Aarhus University) for technical assistance with Western blot analysis and genotyping of mice and Jacob Thygesen for graphical design.

Author Contributions: C.S., M.N., H.E.B., C.A., and V.V.M. contributed to the conception and design of the study. C.S., S.R., J.J., H.C.B., D.A., R.N., and V.V.M. performed the experiments. C.S., N.T.K., P.D.R., C.L., J.P.M., K.L.H., N.R.J., M.N., H.E.B., R.N., and V.V.M. analyzed and interpreted the data. C.S. and V.V.M. prepared the draft and finalized the manuscript. All authors provided critical feedback and approved the final version of the manuscript.

Sources of Funding

This work was supported by the Independent Research Fund Denmark—Medical Sciences (8020-00084B; 9149-00003B) and the Novo Nordisk Foundation (NNF19OC0058460).

Disclosures

None.

Supplemental Material

Tables S1–S2
Figures S1–S10
References 66–84
Data S1–S4

REFERENCES

- Yuen GK, Galice S, Bers DM. Subcellular localization of Na/K-ATPase isoforms in ventricular myocytes. *J Mol Cell Cardiol*. 2017;108:158–169. doi: 10.1016/j.jmcc.2017.05.013
- Berry RG, Despa S, Fuller W, Bers DM, Shattock MJ. Differential distribution and regulation of mouse cardiac Na⁺/K⁺-ATPase alpha1 and alpha2 subunits in t-tubule and surface sarcolemmal membranes. *Cardiovasc Res*. 2007;73:92–100.
- Swift F, Tovsrud N, Enger UH, Sjaastad I, Sejersted OM. The Na⁺/K⁺-ATPase alpha2-isoform regulates cardiac contractility in rat cardiomyocytes. *Cardiovasc Res*. 2007;75:109–117.
- Correll RN, Eder P, Burr AR, Despa S, Davis J, Bers DM, Molkentin JD. Overexpression of the Na⁺/K⁺ ATPase alpha2 but not alpha1 isoform attenuates pathological cardiac hypertrophy and remodeling. *Circ Res*. 2014;114:249–256.
- Despa S, Lingrel JB, Bers DM. Na⁺/K⁺-ATPase alpha2-isoform preferentially modulates Ca²⁺ transients and sarcoplasmic reticulum Ca²⁺ release in cardiac myocytes. *Cardiovasc Res*. 2012;95:480–486.
- Bundgaard H, Kjeldsen K. Human myocardial Na,K-ATPase concentration in heart failure. *Mol Cell Biochem*. 1996;163–164:277–283. doi: 10.1007/BF00408668
- Schwinger RH, Wang J, Frank K, Muller-Ehmsen J, Brixius K, McDonough AA, Erdmann E. Reduced sodium pump alpha1, alpha3, and beta1-isoform protein levels and Na⁺, K⁺-ATPase activity but unchanged Na⁺-Ca²⁺ exchanger protein levels in human heart failure. *Circulation*. 1999;99:2105–2112.
- Nørgaard A, Bagge JP, Bjerregaard P, Baandrup U, Kjeldsen K, Thomsen PE. Relation of left ventricular function and Na,K-pump concentration in suspected idiopathic dilated cardiomyopathy. *Am J Cardiol*. 1988;61:1312–1315. doi: 10.1016/0002-9149(88)91175-7
- Moseley AE, Cougnon MH, Grupp IL, El Schultz J, Lingrel JB. Attenuation of cardiac contractility in Na,K-ATPase alpha1 isoform-deficient hearts under reduced calcium conditions. *J Mol Cell Cardiol*. 2004;37:913–919.
- James PF, Grupp IL, Grupp G, Woo AL, Askew GR, Croyle ML, Walsh RA, Lingrel JB. Identification of a specific role for the Na,K-ATPase alpha 2 isoform as a regulator of calcium in the heart. *Mol Cell*. 1999;3:555–563.
- Chu L, Greenstein JL, Winslow RL. Na⁺ microdomains and sparks: role in cardiac excitation-contraction coupling and arrhythmias in ankyrin-B deficiency. *J Mol Cell Cardiol*. 2019;128:145–157. doi: 10.1016/j.jmcc.2019.02.001
- Skogstad J, Aronsen JM, Tovsrud N, Wanichawan P, Hougen K, Stokke MK, Carlson CR, Sjaastad I, Sejersted OM, Swift F. Coupling of the Na⁺/K⁺-ATPase to ankyrin b controls Na⁺/Ca²⁺ exchanger activity in cardiomyocytes. *Cardiovasc Res*. 2020;116:78–90. doi: 10.1093/cvr/cvz087
- Despa S. Myocyte [Na⁺]_i dysregulation in heart failure and diabetic cardiomyopathy. *Front Physiol*. 2018;9:1303. doi: 10.3389/fphys.2018.01303
- Blaustein MP, Hamlyn JM. Ouabain, endogenous ouabain and ouabain-like factors: the Na⁺ pump/ouabain receptor, its linkage to NCX, and its myriad functions. *Cell Calcium*. 2020;86:102159. doi: 10.1016/j.ceca.2020.102159
- Xie Z. Molecular mechanisms of Na/K-ATPase-mediated signal transduction. *Ann NY Acad Sci*. 2003;986:497–503. doi: 10.1111/j.1749-6632.2003.tb07234.x
- Liu J, Tian J, Haas M, Shapiro JI, Askari A, Xie Z. Ouabain interaction with cardiac Na⁺/K⁺-ATPase initiates signal cascades independent of changes in intracellular Na⁺ and Ca²⁺ concentrations. *J Biol Chem*. 2000;275:27838–27844.
- Wu J, Li D, Du L, Baldawi M, Gable ME, Askari A, Liu L. Ouabain prevents pathological cardiac hypertrophy and heart failure through activation of phosphoinositide 3-kinase alpha in mouse. *Cell Biosci*. 2015;5:64.
- Yan X, Xun M, Dou X, Wu L, Zhang F, Zheng J. Activation of Na⁺-K⁺-ATPase with DRm217 attenuates oxidative stress-induced myocardial cell injury via closing Na⁺-K⁺-ATPase/Src/Ros amplifier. *Apoptosis*. 2017;22:531–543. doi: 10.1007/s10495-016-1342-2
- Li Z, Cai T, Tian J, Xie JX, Zhao X, Liu L, Shapiro JI, Xie Z. Naktide, a Na⁺/K-ATPase-derived peptide Src inhibitor, antagonizes Ouabain-activated signal transduction in cultured cells. *J Biol Chem*. 2009;284:21066–21076. doi: 10.1074/jbc.M109.013821
- Galougahi KK, Liu CC, Bundgaard H, Rasmussen HH. Beta-adrenergic regulation of the cardiac Na⁺-K⁺ ATPase mediated by oxidative signaling. *Trends Cardiovasc Med*. 2012;22:83–87.
- Liu J, Nie Y, Chaudhry M, Bai F, Chuang J, Sodhi K, Shapiro JI. The redox-sensitive Na/K-ATPase signaling in uremic cardiomyopathy. *Int J Mol Sci*. 2020;21:1256. doi: 10.3390/ijms21041256
- Liu J, Tian J, Chaudhry M, Maxwell K, Yan Y, Wang X, Shah PT, Khawaja AA, Martin R, Robinette TJ, et al. Attenuation of Na/K-ATPase mediated oxidant amplification with pNaktide ameliorates experimental uremic cardiomyopathy. *Sci Rep*. 2016;6:34592. doi: 10.1038/srep34592
- De Fusco M, Marconi R, Silvestri L, Atorino L, Rampoldi L, Morgante L, Ballabio A, Aridon P, Casari G. Haploinsufficiency of ATP1a2 encoding the Na⁺/K⁺ pump alpha2 subunit associated with familial hemiplegic migraine type 2. *Nat Genet*. 2003;33:192–196.
- Adelborg K, Szépligeti SK, Holland-Bill L, Ehrenstein V, Horváth-Puhó E, Henderson VW, Sørensen HT. Migraine and risk of cardiovascular diseases: Danish population based matched cohort study. *BMJ*. 2018;360:k96. doi: 10.1136/bmj.k96
- Böttger P, Glerup S, Gesslein B, Illarionova NB, Isaksen TJ, Heuck A, Clausen BH, Füchtbauer EM, Gramsbergen JB, Gunnarson E, et al. Glutamate-system defects behind psychiatric manifestations in a familial hemiplegic migraine type 2 disease-mutation mouse model. *Sci Rep*. 2016;6:22047. doi: 10.1038/srep22047
- Spadaro M, Ursu S, Lehmann-Horn F, Veneziano L, Antonini G, Giunti P, Frontali M, Jurkat-Rott K. A G301R Na⁺/K⁺-ATPase mutation causes familial hemiplegic migraine type 2 with cerebellar signs. *Neurogenetics*. 2004;5:177–185. doi: 10.1007/s10048-004-0183-2
- Staehr C, Hangaard L, Bouzinova EV, Kim S, Rajanathan R, Boegh Jessen P, Luque N, Xie Z, Lykke-Hartmann K, Sandow SL, et al. Smooth muscle Ca(2+) sensitization causes hypercontractility of middle cerebral arteries in mice bearing the familial hemiplegic migraine type 2 associated mutation. *J Cereb Blood Flow Metab*. 2018;39:1570–1587.
- Staehr C, Rajanathan R, Postnov DD, Hangaard L, Bouzinova EV, Lykke-Hartmann K, Bach FW, Sandow SL, Aalkjaer C, Matchkov VV. Abnormal neurovascular coupling as a cause of excess cerebral vasodilation in familial migraine. *Cardiovasc Res*. 2019;116:2009–2020. doi: 10.1093/cvr/cvz306
- Tzur A, Kafri R, LeBleu VS, Lahav G, Kirschner MW. Cell growth and size homeostasis in proliferating animal cells. *Science*. 2009;325:167–171. doi: 10.1126/science.1174294
- Grist JT, Mariager CO, Qi H, Nielsen PM, Laustsen C. Detection of acute kidney injury with hyperpolarized [(13)C], (15)N]urea and multiexponential relaxation modeling. *Magn Reson Med*. 2019;84:943–949.
- Hill DK, Orton MR, Mariotti E, Boulton JK, Panek R, Jafar M, Parkes HG, Jamin Y, Miniotti MF, Al-Saffar NM, et al. Model free approach to kinetic analysis of real-time hyperpolarized 13C magnetic resonance spectroscopy data. *PLoS One*. 2013;8:e71996. doi: 10.1371/journal.pone.0071996
- Jensen AB, Joergensen HB, Dam VS, Kamaev D, Boedtker D, Füchtbauer EM, Aalkjaer C, Matchkov VV. Variable contribution of TMEM16A to tone in murine arterial vasculature. *Basic Clin Pharmacol Toxicol*. 2018;123:30–41. doi: 10.1111/bcpt.12984
- Corydon KK, Matchkov V, Fais R, Abramochkin D, Hedegaard ER, Comerma-Steffensen S, Simonsen U. Effect of ischemic preconditioning and a Kv7 channel blocker on cardiac ischemia-reperfusion injury in rats. *Eur J Pharmacol*. 2020;866:172820. doi: 10.1016/j.ejphar.2019.172820
- Lang D, Glukhov AV. High-resolution optical mapping of the mouse sino-atrial node. *J Vis Exp*. 2016:54773. doi: 10.3791/54773
- Christiansen LB, Dela F, Koch J, Hansen CN, Leifsson PS, Yokota T. Impaired cardiac mitochondrial oxidative phosphorylation and enhanced mitochondrial oxidative stress in feline hypertrophic cardiomyopathy. *Am J Physiol Heart Circ Physiol*. 2015;308:H1237–H1247. doi: 10.1152/ajpheart.00727.2014
- Jespersen NR, Yokota T, Stottrup NB, Bergdahl A, Paelestik KB, Povlsen JA, Dela F, Bøtker HE. Pre-ischaemic mitochondrial substrate constraint by inhibition of malate-aspartate shuttle preserves mitochondrial function after ischaemia-reperfusion. *J Physiol*. 2017;595:3765–3780. doi: 10.1113/JP273408
- Lanza IR, Nair KS. Functional assessment of isolated mitochondria in vitro. *Methods Enzymol*. 2009;457:349–372.
- Matchkov VV, Kravtsova VV, Wiborg O, Aalkjaer C, Bouzinova EV. Chronic selective serotonin reuptake inhibition modulates endothelial dysfunction and oxidative state in rat chronic mild stress model of depression.

- Am J Physiol Regul Integr Comp Physiol.* 2015;309:R814–R823. doi: 10.1152/ajpregu.00337.2014
39. Behr Andersen C, Lindholt JS, Urbonavicius S, Halekoh U, Jensen PS, Stubbe J, Rasmussen LM, Beck HC. Abdominal aortic aneurysms growth is associated with high concentrations of plasma proteins in the intraluminal thrombus and diseased arterial tissue. *Arterioscler Thromb Vasc Biol.* 2018;38:2254–2267. doi: 10.1161/ATVBAHA.117.310126
 40. Perez-Riverol Y, Csordas A, Bai J, Bernal-Llinares M, Hewapathirana S, Kundu DJ, Inuganti A, Griss J, Mayer G, Eisenacher M, et al. The pride database and related tools and resources in 2019: improving support for quantification data. *Nucleic Acids Res.* 2019;47:D442–D450. doi: 10.1093/nar/gky1106
 41. Shinoda T, Ogawa H, Cornelius F, Toyoshima C. Crystal structure of the sodium-potassium pump at 2.4 Å resolution. *Nature.* 2009;459:446–450.
 42. Sali A, Blundell TL. Comparative protein modelling by satisfaction of spatial restraints. *J Mol Biol.* 1993;234:779–815. doi: 10.1006/jmbi.1993.1626
 43. Webb B, Sali A. Comparative protein structure modeling using MODELLER. *Curr Protoc Bioinformatics.* 2014;47:1–32. doi: 10.1002/0471250953.bi0506s47
 44. Brand MD, Nicholls DG. Assessing mitochondrial dysfunction in cells. *Biochem J.* 2011;435:297–312. doi: 10.1042/BJ20110162
 45. Larsen S, Nielsen J, Hansen CN, Nielsen LB, Wibrand F, Stride N, Schroder HD, Boushel R, Helge JW, Dela F, et al. Biomarkers of mitochondrial content in skeletal muscle of healthy young human subjects. *J Physiol.* 2012;590:3349–3360. doi: 10.1113/jphysiol.2012.230185
 46. Rajabi M, Kassiotis C, Razeghi P, Taegtmeier H. Return to the fetal gene program protects the stressed heart: a strong hypothesis. *Heart Fail Rev.* 2007;12:331–343. doi: 10.1007/s10741-007-9034-1
 47. Tran DH, Wang ZV. Glucose metabolism in cardiac hypertrophy and heart failure. *J Am Heart Assoc.* 2019;8:e012673. doi: 10.1161/JAHA.119.012673
 48. Chance B, Sies H, Boveris A. Hydroperoxide metabolism in mammalian organs. *Physiol Rev.* 1979;59:527–605. doi: 10.1152/physrev.1979.59.3.527
 49. Stepanov AV, Baidyuk EV, Sakuta GA. The features of mitochondria of cardiomyocytes from rats with chronic heart failure. *Cell Tissue Biol.* 2017;11:458–465. doi: 10.1134/S1990519X17060086
 50. Collins HE, Kane MS, Litovsky SH, Darley-Usmar VM, Young ME, Chatham JC, Zhang J. Mitochondrial morphology and mitophagy in heart diseases: qualitative and quantitative analyses using transmission electron microscopy. *Front Aging.* 2021;2:670267. doi: 10.3389/fragi.2021.670267
 51. Heusch G, Boengler K, Schulz R. Inhibition of mitochondrial permeability transition pore opening: the holy grail of cardioprotection. *Basic Res Cardiol.* 2010;105:151–154. doi: 10.1007/s00395-009-0080-9
 52. Clarke SJ, Khalilul I, Das M, Parker JE, Heesom KJ, Halestrap AP. Inhibition of mitochondrial permeability transition pore opening by ischemic preconditioning is probably mediated by reduction of oxidative stress rather than mitochondrial protein phosphorylation. *Circ Res.* 2008;102:1082–1090. doi: 10.1161/CIRCRESAHA.107.167072
 53. Yan Y, Shapiro AP, Haller S, Katragadda V, Liu L, Tian J, Basur V, Malhotra D, Xie ZJ, Abraham NG, et al. Involvement of reactive oxygen species in a feed-forward mechanism of Na/K-ATPase-mediated signaling transduction. *J Biol Chem.* 2013;288:34249–34258. doi: 10.1074/jbc.M113.461020
 54. Bartlett DE, Miller RB, Thiesfeldt S, Lakhani HV, Shapiro JI, Sodhi K. The role of Na/K-ATPase signaling in oxidative stress related to aging: implications in obesity and cardiovascular disease. *Int J Mol Sci.* 2018;19:2139. doi: 10.3390/ijms19072139
 55. Canton M, Menazza S, Sheeran FL, Poverino de Laureto P, Di Lisa F, Pepe S. Oxidation of myofibrillar proteins in human heart failure. *J Am Coll Cardiol.* 2011;57:300–309. doi: 10.1016/j.jacc.2010.06.058
 56. Canton M, Skyschally A, Menabò R, Boengler K, Gres P, Schulz R, Haude M, Erbel R, Di Lisa F, Heusch G. Oxidative modification of tropomyosin and myocardial dysfunction following coronary microembolization. *Eur Heart J.* 2006;27:875–881. doi: 10.1093/eurheartj/ehi751
 57. Kociol RD, Pang PS, Gheorghiade M, Fonarow GC, O'Connor CM, Felker GM. Troponin elevation in heart failure prevalence, mechanisms, and clinical implications. *J Am Coll Cardiol.* 2010;56:1071–1078. doi: 10.1016/j.jacc.2010.06.016
 58. Rindler TN, Dostanic I, Lasko VM, Nieman ML, Neumann JC, Lorenz JN, Lingrel JB. Knockout of the Na,K-ATPase alpha(2)-isoform in the cardiovascular system does not alter basal blood pressure but prevents aortic-induced hypertension. *Am J Physiol.* 2011;301:H1396–H1404.
 59. Chen L, Song H, Wang Y, Lee JC, Kottikoff MI, Pritchard TJ, Paul RJ, Zhang J, Blaustein MP. Arterial alpha2-Na⁺ pump expression influences blood pressure: lessons from novel, genetically engineered smooth muscle-specific alpha2 mice. *Am J Physiol.* 2015;309:H958–H968.
 60. Yamamoto T, Su Z, Moseley AE, Kadono T, Zhang J, Cougnon M, Li F, Lingrel JB, Barry WH. Relative abundance of alpha2 Na⁺ pump isoform influences Na⁺-Ca²⁺ exchanger currents and Ca²⁺ transients in mouse ventricular myocytes. *J Mol Cell Cardiol.* 2005;39:113–120.
 61. Magyar CE, Wang J, Azuma KK, McDonough AA. Reciprocal regulation of cardiac Na-K-ATPase and Na/Ca exchanger: hypertension, thyroid hormone, development. *Am J Physiol.* 1995;269:C675–C682. doi: 10.1152/ajpcell.1995.269.3.C675
 62. Matchkov VV, Moeller-Nielsen N, Dam VS, Nourian Z, Briggs Boedtker DM, Aalkjaer C. The alpha2 isoform of the Na,K-pump is important for intercellular communication, agonist-induced contraction and EDHF-like response in rat mesenteric arteries. *Am J Physiol.* 2012;303:H36–H46.
 63. Sodhi K, Nichols A, Mallick A, Klug RL, Liu J, Wang X, Srikanth K, Goguet-Rubio P, Nawab A, Pratt R, et al. The Na/K-ATPase oxidant amplification loop regulates aging. *Sci Rep.* 2018;8:9721. doi: 10.1038/s41598-018-26768-9
 64. Liu CC, Fry NA, Hamilton EJ, Chia KK, Garcia A, Karimi Galougahi K, Fittree GA, Clarke RJ, Bundgaard H, Rasmussen HH. Redox-dependent regulation of the Na⁺-K⁺ pump: new twists to an old target for treatment of heart failure. *J Mol Cell Cardiol.* 2013;61:94–101. doi: 10.1016/j.jmcc.2013.05.013
 65. Bottger P, Doganli C, Lykke-Hartmann K. Migraine- and dystonia-related disease-mutations of Na⁺/K⁺-ATPases: relevance of behavioral studies in mice to disease symptoms and neurological manifestations in humans. *Neurosci Biobehav Rev.* 2012;36:855–871.
 66. Ahmad F, Banerjee SK, Lage ML, Huang XN, Smith SH, Saba S, Rager J, Conner DA, Janczewski AM, Tobita K, et al. The role of cardiac troponin T quantity and function in cardiac development and dilated cardiomyopathy. *PLoS One.* 2008;3:e2642. doi: 10.1371/journal.pone.0002642
 67. McKeown CR, Nowak RB, Gokhin DS, Fowler VM. Tropomyosin is required for cardiac morphogenesis, myofibril assembly, and formation of adherens junctions in the developing mouse embryo. *Dev Dyn.* 2014;243:800–817. doi: 10.1002/dvdy.24115
 68. Layland J, Solaro RJ, Shah AM. Regulation of cardiac contractile function by troponin I phosphorylation. *Cardiovasc Res.* 2005;66:12–21. doi: 10.1016/j.cardiores.2004.12.022
 69. Mudry RE, Perry CN, Richards M, Fowler VM, Gregorio CC. The interaction of tropomodulin with tropomyosin stabilizes thin filaments in cardiac myocytes. *J Cell Biol.* 2003;162:1057–1068. doi: 10.1083/jcb.200305031
 70. Carrier L, Mearini G, Stathopoulou K, Cuervo F. Cardiac myosin-binding protein C (MYBPC3) in cardiac pathophysiology. *Gene.* 2015;573:188–197. doi: 10.1016/j.gene.2015.09.008
 71. Cui Y, Zheng Y, Liu X, Yan L, Fan X, Yong J, Hu Y, Dong J, Li Q, Wu X, et al. Single-cell transcriptome analysis maps the developmental track of the human heart. *Cell Rep.* 2019;26:1934–1950.e5. doi: 10.1016/j.celrep.2019.01.079
 72. Guo Y, Pu WT. Cardiomyocyte maturation: new phase in development. *Circ Res.* 2020;126:1086–1106. doi: 10.1161/CIRCRESAHA.119.315862
 73. Parlakian A, Charvet C, Escoubet B, Mericskay M, Molkentin JD, Gary-Bobo G, De Windt LJ, Ludovsky MA, Paulin D, Daegelen D, et al. Temporally controlled onset of dilated cardiomyopathy through disruption of the SRF gene in adult heart. *Circulation.* 2005;112:2930–2939.
 74. Kooij V, Viswanathan MC, Lee DI, Rainer PP, Schmidt W, Kronert WA, Harding SE, Kass DA, Bernstein SL, Van Eyk JE, et al. Profilin modulates sarcomeric organization and mediates cardiomyocyte hypertrophy. *Cardiovasc Res.* 2016;110:238–248. doi: 10.1093/cvr/cvv050
 75. Luther DJ, Thodeti CK, Shamhart PE, Adapala RK, Hodnichak C, Weihrach D, Bonaldo P, Chilian WM, Meszaros JG. Absence of type VI collagen paradoxically improves cardiac function, structure, and remodeling after myocardial infarction. *Circ Res.* 2012;110:851–856. doi: 10.1161/CIRCRESAHA.111.252734
 76. Sack MN. Rab4a signaling unmasks a pivotal link between myocardial homeostasis and metabolic remodeling in the diabetic heart. *J Mol Cell Cardiol.* 2010;49:908–910. doi: 10.1016/j.jmcc.2010.09.002
 77. Battelli MG, Polito L, Bortolotti M, Bolognesi A. Xanthine oxidoreductase-derived reactive species: physiological and pathological effects. *Oxid Med Cell Longev.* 2016;2016:3527579. doi: 10.1155/2016/3527579

78. Munzel T, Camici GG, Maack C, Bonetti NR, Fuster V, Kovacic JC. Impact of oxidative stress on the heart and vasculature: part 2 of a 3-part series. *J Am Coll Cardiol*. 2017;70:212–229.
79. Nagano T, Nakashima A, Onishi K, Kawai K, Awai Y, Kinugasa M, Iwasaki T, Kikkawa U, Kamada S. Proline dehydrogenase promotes senescence through the generation of reactive oxygen species. *J Cell Sci*. 2017;130:1413–1420.
80. Huang Q, Zhou HJ, Zhang H, Huang Y, Hinojosa-Kirschenbaum F, Fan P, Yao L, Belardinelli L, Tellides G, Giordano FJ, et al. Thioredoxin-2 inhibits mitochondrial reactive oxygen species generation and apoptosis stress kinase-1 activity to maintain cardiac function. *Circulation*. 2015;131:1082–1097. doi: 10.1161/CIRCULATIONAHA.114.012725
81. Pahwa S, Sharma R, Singh B. Role of glutathione s-transferase in coronary artery disease patients with and without type 2 diabetes mellitus. *J Clin Diagn Res*. 2017;11:BC05–BC08. doi: 10.7860/JCDR/2017/23846.9281
82. Oppermann U. Carbonyl reductases: the complex relationships of mammalian carbonyl- and quinone-reducing enzymes and their role in physiology. *Annu Rev Pharmacol Toxicol*. 2007;47:293–322. doi: 10.1146/annurev.pharmtox.47.120505.105316
83. van der Pol A, Gil A, Silljé HHW, Tromp J, Ovchinnikova ES, Vreeswijk-Baudoin I, Hoes M, Domian IJ, van de Sluis B, van Deursen JM, et al. Accumulation of 5-oxoproline in myocardial dysfunction and the protective effects of OPLAH. *Sci Transl Med*. 2017;9. doi: 10.1126/scitranslmed.aam8574
84. Hendgen-Cotta UB, Kelm M, Rassaf T. Myoglobin functions in the heart. *Free Radic Biol Med*. 2014;73:252–259. doi: 10.1016/j.freeradbiomed.2014.05.005

SUPPLEMENTAL MATERIAL

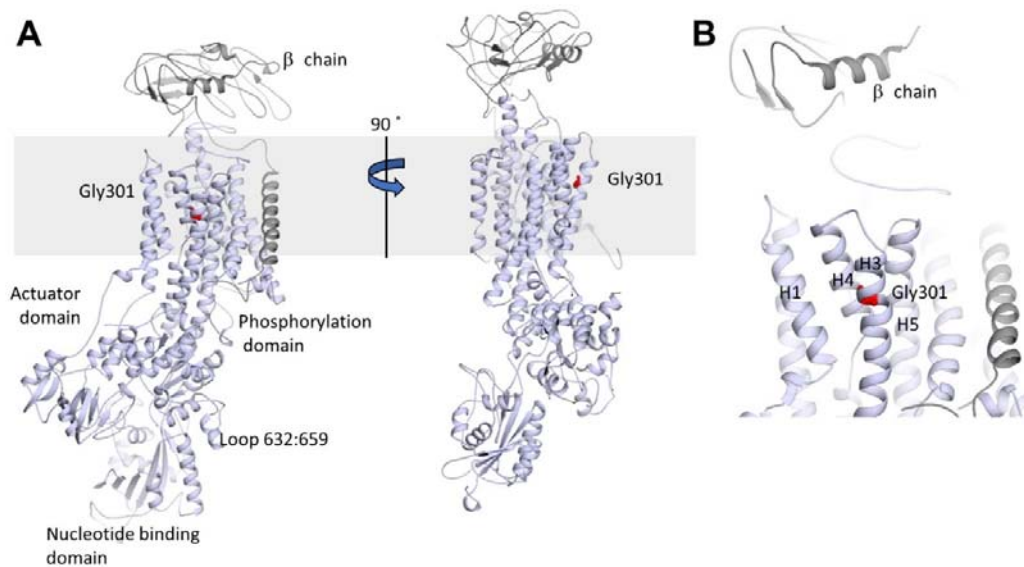
Table S1. Basic information and supplementary findings from cardiac magnetic resonance imaging of $\alpha_2^{+/G301R}$ and wild type mice. Data are shown as mean \pm standard mean error. *, $P < 0.05$ (unpaired t -test).

3-month-old mice			
	wild type ($n = 6$)	$\alpha_2^{+/G301R}$ ($n = 6$)	P value
Body weight (g)	20.02 \pm 0.66	17.83 \pm 1.19	0.14
Heart rate (min^{-1})	434.9 \pm 35.3	443.0 \pm 20.6	0.85
Respiration frequency (min^{-1})	147.3 \pm 13.4	163.3 \pm 5.6	0.30
Left ventricular end-diastolic volume (ml)	0.051 \pm 0.005	0.047 \pm 0.004	0.57
Left ventricular end-systolic volume (ml)	0.014 \pm 0.002	0.016 \pm 0.002	0.60
Left ventricular ejection fraction (%)	71.99 \pm 2.09	66.52 \pm 2.47	0.12
Left ventricular stroke volume ($\text{ml} \cdot \text{beat}^{-1}$)	0.036 \pm 0.004	0.031 \pm 0.002	0.25
Left ventricular cardiac output ($\text{ml} \cdot \text{min}^{-1}$)	15.90 \pm 2.31	13.53 \pm 0.62	0.35
Left ventricular cardiac index ($\text{ml} \cdot \text{min}^{-1} \cdot \text{g}^{-1}$)	0.793 \pm 0.107	0.772 \pm 0.051	0.87
Left ventricular mass-to-body weight ratio ($\text{mm}^3 \cdot \text{g}^{-1}$)	3.844 \pm 0.183	3.384 \pm 0.174	0.10
Right ventricular end-diastolic volume (ml)	0.041 \pm 0.003	0.038 \pm 0.003	0.46
Right ventricular end systolic volume (ml)	0.011 \pm 0.002	0.009 \pm 0.001	0.74
Right ventricular ejection fraction (%)	74.66 \pm 3.63	74.17 \pm 1.95	0.91
8-month-old mice			
	wild type ($n = 7$)	$\alpha_2^{+/G301R}$ ($n = 10$)	P value
Body weight (g)	27.96 \pm 1.35	29.86 \pm 1.23	0.32
Heart rate (min^{-1})	485.0 \pm 30.6	434.1 \pm 12.5	0.10
Respiration frequency (min^{-1})	132.6 \pm 6.7	147.4 \pm 11.4	0.13
Left ventricular diastolic volume (ml)	0.064 \pm 0.006	0.080 \pm 0.004	0.04*
Left ventricular systolic volume (ml)	0.017 \pm 0.003	0.026 \pm 0.003	0.03*
Left ventricular ejection fraction (%)	75.18 \pm 2.57	67.09 \pm 1.81	0.02*
Left ventricular stroke volume ($\text{ml} \cdot \text{beat}^{-1}$)	0.048 \pm 0.004	0.053 \pm 0.003	0.20
Left ventricular cardiac output ($\text{ml} \cdot \text{min}^{-1}$)	23.24 \pm 1.66	22.90 \pm 1.91	0.87
Left ventricular cardiac index ($\text{ml} \cdot \text{min}^{-1} \cdot \text{g}^{-1}$)	0.837 \pm 0.058	0.783 \pm 0.062	0.55
Left ventricular mass-to-body weight ratio ($\text{mm}^3 \cdot \text{g}^{-1}$)	3.325 \pm 0.170	3.432 \pm 0.130	0.62
Right ventricular diastolic volume (ml)	0.040 \pm 0.005	0.053 \pm 0.002	0.02*
Right ventricular systolic volume (ml)	0.013 \pm 0.003	0.017 \pm 0.002	0.20
Right ventricular ejection fraction (%)	73.49 \pm 3.52	69.59 \pm 1.95	0.31

Table S2. Characteristics of spontaneous electrical activity of atrial and ventricular myocardium from 8-month-old $\alpha_2^{+/G301R}$ and wild type mice. APD50 and APD90 indicate action potential duration at the level of 50% and 90% repolarization. Data are shown as mean \pm standard mean error. Groups were compared using unpaired *t*-test. See also Figure S3 for representative traces of membrane potentials.

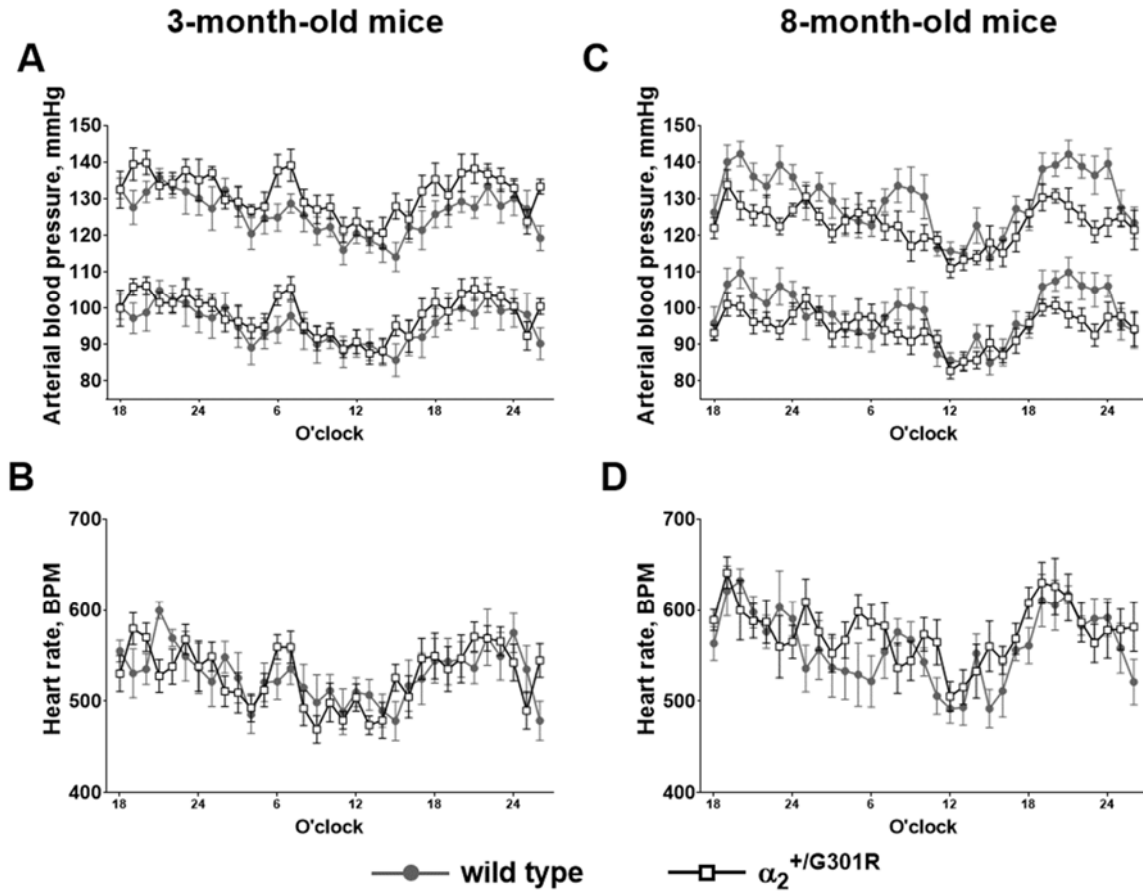
	Wild type (<i>n</i> = 9)	$\alpha_2^{+/G301R}$ (<i>n</i> = 8)	<i>P</i> value
Right ventricle wall			
Heart rate (min ⁻¹)	404.0 \pm 11.9	422.2 \pm 20.4	0.44
Resting membrane potential (mV)	-80.9 \pm 1.0	-79.9 \pm 1.5	0.54
Resting potential interval (ms)	147.3 \pm 5.3	144.6 \pm 4.8	0.71
APD50 (ms)	8.79 \pm 0.70	8.43 \pm 0.44	0.68
APD90 (ms)	33.02 \pm 2.48	32.62 \pm 2.13	0.91
Action potential amplitude (mV)	109.5 \pm 2.3	109.9 \pm 2.8	0.92
Maximal depolarization (mV)	30.4 \pm 1.9	28.6 \pm 1.5	0.46
Maximal slope of depolarization (mV/s)	375320 \pm 27989	365007 \pm 23912	0.78
Right atrial trabeculae			
Heart rate (/min)	409.3 \pm 12.7	423.9 \pm 13.4	0.44
Resting membrane potential (mV)	-83.1 \pm 0.8	-83.4 \pm 1.8	0.85
Resting potential interval (ms)	144.2 \pm 4.0	143.8 \pm 4.1	0.94
APD50 (ms)	11.52 \pm 1.84	10.44 \pm 0.45	0.66
APD90 (ms)	23.91 \pm 2.19	28.64 \pm 2.61	0.18
Action potential amplitude (mV)	115.6 \pm 1.8	110.8 \pm 3.9	0.25
Maximal depolarization (mV)	32.5 \pm 1.4	29.8 \pm 2.3	0.31
Maximal slope of depolarization (mV/s)	313687 \pm 9511	317438 \pm 27078	0.88
Right atrial wall			
Heart rate (/min)	416.9 \pm 13.9	424.2 \pm 15.4	0.73
Resting membrane potential (mV)	-82.0 \pm 0.9	-83.3 \pm 1.4	0.43
Resting potential interval (ms)	143.1 \pm 3.7	142.8 \pm 4.4	0.95
APD50 (ms)	5.74 \pm 0.83	5.36 \pm 0.54	0.71
APD90 (ms)	15.44 \pm 2.25	17.93 \pm 0.95	0.35
Action potential amplitude (mV)	104.5 \pm 2.1	101.1 \pm 2.8	0.34
Maximal depolarization (mV)	22.3 \pm 1.5	17.3 \pm 2.3	0.08
Maximal slope of depolarization (mV/s)	247597 \pm 18311	230319 \pm 17148	0.51
Right atrial posterior part of intercaval region			
Heart rate (/min)	411.2 \pm 15.3	449.1 \pm 32.3	0.29
Resting membrane potential (mV)	-83.3 \pm 0.9	-84.7 \pm 1.2	0.37
Resting potential interval (ms)	145.3 \pm 3.9	140.3 \pm 4.5	0.40
APD50 (ms)	12.88 \pm 1.87	11.10 \pm 0.88	0.42
APD90 (ms)	34.19 \pm 3.26	31.26 \pm 2.22	0.48
Action potential amplitude (mV)	106.1 \pm 1.9	108.9 \pm 2.1	0.34
Maximal depolarization (mV)	25.2 \pm 1.8	23.2 \pm 1.9	0.47
Maximal slope of depolarization (mV/s)	234844 \pm 16919	278884 \pm 23057	0.14

Figure S1.



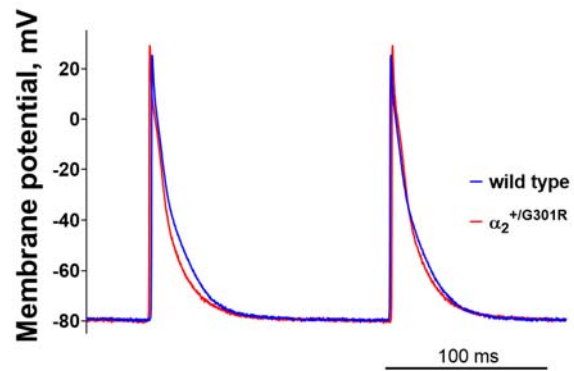
A homology model of the human Na,K-ATPase $\alpha 2$ isoform (light blue) and the β isoform 1 (grey) is shown as cartoon representation from two different angles, rotated 90 degrees (A). The Familial Hemiplegic Migraine type 2-associated Gly301Arg25 mutation is plotted on the homology model and highlighted in red. A close up of the structural region around the mutation (B) show that Gly301Arg mutation is located in transmembrane helix (H3) and might interfere with the membrane helix arrangement around transmembrane helices 1, 4 and 5 (H1, H4, H5).

Figure S2.



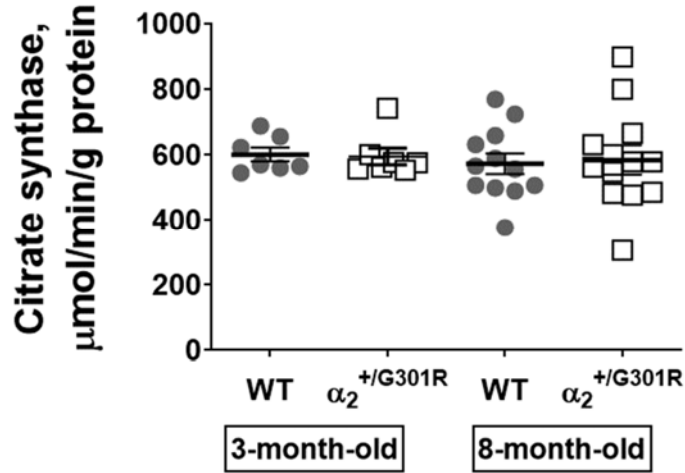
Circadian variations in blood pressure (A, C) and heart rate (B, D) of 3-month-old (A, B; $n = 6 - 9$) and 8-month-old (C, D; $n = 7$) $\alpha_2^{+/G301R}$ and wild type mice. For statistical analyses, see Figure 3.

Figure S3.



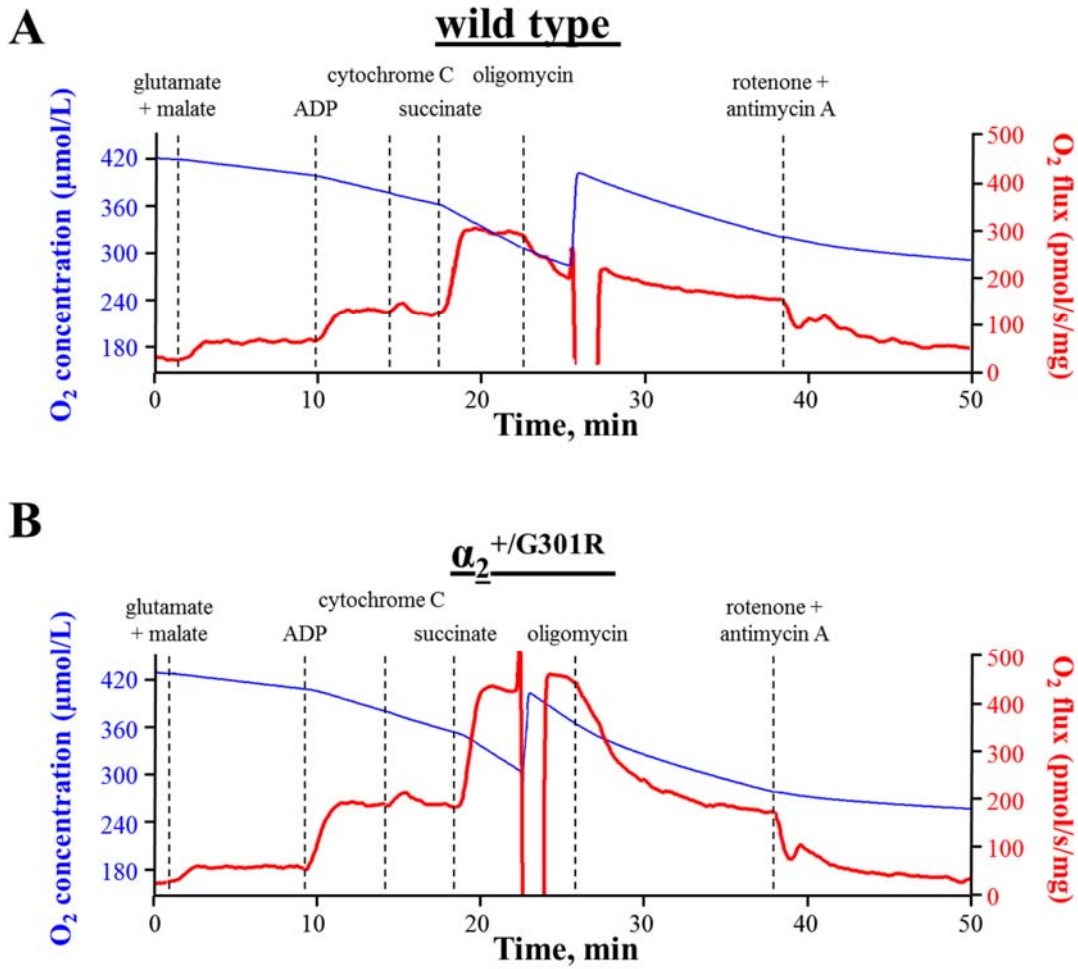
Representative traces of membrane potentials show that the waveform of spontaneous left ventricle membrane action potentials recorded in ventricular myocardium was similar in the hearts from $\alpha_2^{+/G301R}$ and wild type mice. See Table S2 for statistical analyses.

Figure S4.



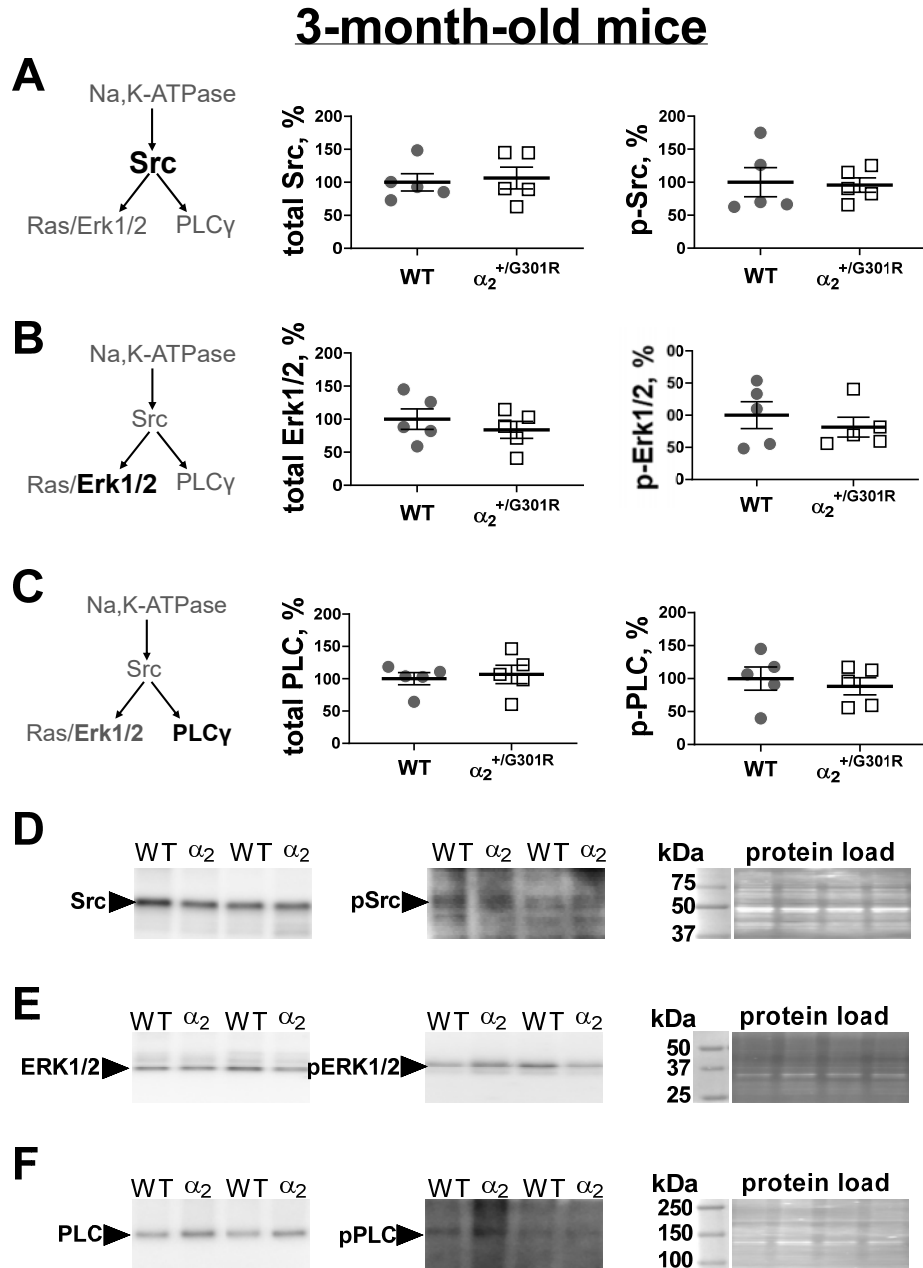
Citrate synthase activity as a marker enzyme for mitochondrial content suggested similar mitochondrial content in cardiac samples from 3-month-old ($n = 7$) and 8-month-old ($n = 12$) $\alpha_2^{+/G301R}$ and wild type mice. Data compared with two-way ANOVA.

Figure S5.



Representative respirometry traces of hearts from 8-month-old wild type (A) and $\alpha_2^{+/G301R}$ (B) mice. Blue traces show O_2 concentration (hyperoxygenated environment), red traces show O_2 consumption.

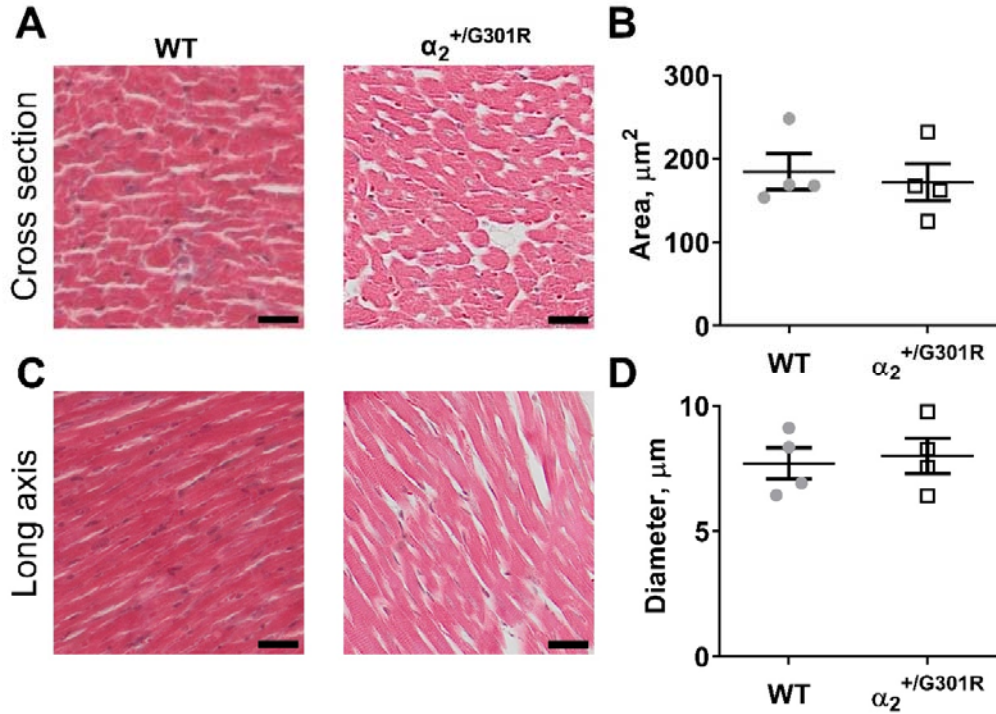
Figure S6. Phospho-specific Western blot analysis did not suggest any changes in the expression of key molecules for the Na,K-ATPase-dependent signalling pathways in the hearts from 3-month-old $\alpha_2^{+/G301R}$ and wild type mice.



Semi-quantitative assessment of total Src kinase expression and the level of Src phosphorylation at Tyr418 (A), total Erk1/2 kinase expression and its Thr202/Tyr204 phosphorylation level (B), and total PLCγ expression and the level of its Tyr783 phosphorylation (C). Representative images for Src

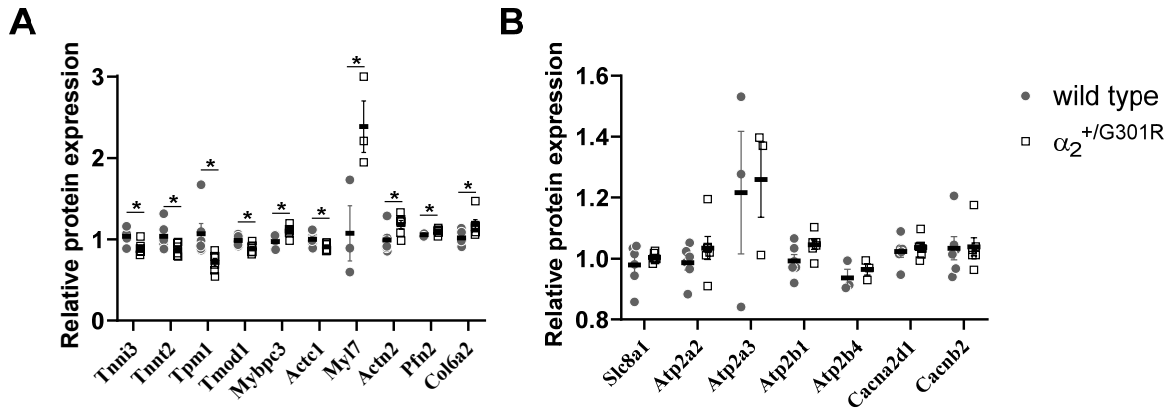
(D), Erk1/2 (E), and PLC γ (F) semi-quantification Western blot experiments that are averaged in (A), (B) and (C), respectively. Left images correspond to total protein-of-interest (Src, Erk1/2 and PLC γ , respectively). Images in the center correspond to phosphorylated protein of interest (p-Src, p-Erk1/2 and p-PLC γ , respectively). Molecular weight markers and total protein load in the membrane detected with stain-free gels are shown to the right. All representative images were cropped to the size identified by molecular marker in (D), (E) and (F), respectively. All images are cropped to include at three molecular weight markers positioned both above and below the band. Prior to incubation with the antibodies, the membrane was divided into two parts; the upper part above 75 kDa was used to detect PLC γ and p-PLC γ , the lower part below 75 kDa was used to detect either Src and p-Src, or Erk1/2 and p-Erk1/2, respectively. The expression was normalized to total protein load for the corresponding probe. An average level for the wild type (WT) group was taken as 100%. $n = 5$. Data compared with unpaired t -test.

Figure S7. Morphology of left ventricle tissue was similar in 8-month-old mice of both genotypes.



Masson's trichrome staining of left ventricle cross sections. Cytoplasm and muscle fibres appear red, nuclei are blue. The tissue was examined at x20 magnification. Representative images of myocardium with cardiomyocytes in cross sectional orientation from a wild type (WT) and $\alpha_2^{+/G301R}$ mouse (A). The area of cardiomyocytes in the cross-sectional orientation was similar between genotypes (B). Representative images of cardiomyocytes in long axis (C). Cardiomyocyte diameter measured in long-axis was similar between genotypes (D). No fibrosis was detected in the myocardium in any of the mice of both genotypes. $n = 4$. Bars in (A and C) correspond to 30 μm . Data compared with unpaired t -test.

Figure S8. Systolic dysfunction in 8-month-old $\alpha_2^{+/G301R}$ mice may be a result of changes in the contractile machinery but not of Ca^{2+} handling.

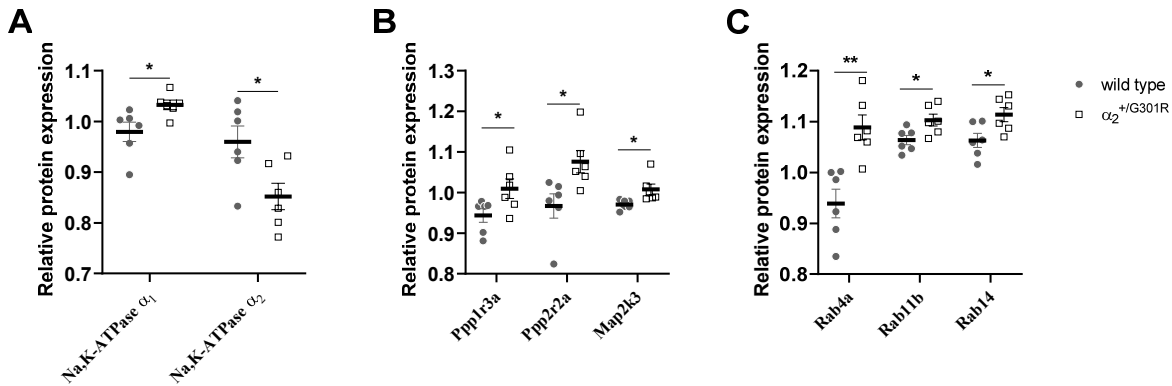


(A) The expression of several proteins important for the Ca^{2+} -dependent interaction of actin and myosin during cardiomyocyte contraction was modified in $\alpha_2^{+/G301R}$ hearts, including suppressed components of the troponin-tropomyosin complex i.e. cardiac troponin I3 (Tnni3), troponin T2 (Tnni2), α -tropomyosin (Tpm1) and tropomodulin 1 (Tmod1). Reduced Tnni2 was previously suggested to contribute to dilated cardiomyopathy-like changes in the mouse heart.⁶⁶ An ablation of Tpm1 was shown to lead to degeneration of partially assembled sarcomeres due to unregulated actin-myosin interactions⁶⁷ and its abnormal regulation is associated with dilated cardiomyopathy.⁶⁸ Tmod1 is also essential for regulation of the thin filament elongation and depolymerization.⁶⁹ Moreover, cardiac myosin-binding protein C (Mybpc3) is the thick filament associated protein that mediates regulation of acto-myosin cross-bridge cycling, i.e., regulation of cardiac contraction and relaxation.⁷⁰ Mutations in Mybpc3 are associated with a large range of inherited cardiomyopathies. It has been shown that Mybpc3 haploinsufficiency leads to increased myofilament Ca^{2+} sensitivity. It is therefore possible that increased Mybpc3 expression, as it is seen in $\alpha_2^{+/G301R}$ mice, is associated with a reduction in Ca^{2+} sensitivity of the myofilaments and contractility. Accordingly, the upregulation of myosin light chain 7 (Myl7), reduction of Tnni3 and increase in α -actinin 2 (Actn2)⁷¹ are characteristic for the hearts with low Ca^{2+} sensitivity.^{71, 72} Reduction in cardiac α -actin (Actc1), a major constituent of the cytoskeleton of cardiomyocytes, is associated with dilated cardiomyopathy⁷³. Profilin 2 (Pfn2), an actin-binding protein involved in the dynamic turnover of the actin cytoskeleton, was increased in $\alpha_2^{+/G301R}$ cardiomyocytes. Pfn2 is known to modulate the sarcomere structure, partially via Erk1/2 signalling⁷⁴ that, accordingly, was increased in 8-month-

old $\alpha_2^{+/G301R}$ mice (Fig. 6). An increased expression of collagen type VI α_2 chain (Col6a2) was previously associated with worsened cardiac function and remodelling.⁷⁵

(B) No difference in the Ca^{2+} transporting proteins was seen between the hearts from 8-month-old $\alpha_2^{+/G301R}$ and wild type (WT) mice. The similar expression of the Na,Ca-exchanger 1 (Slc8a1), the sarcoplasmic/endoplasmic reticulum Ca^{2+} ATPase 2 (Atp2a2) and 3 (Atp2a3), the plasma membrane Ca^{2+} -transporting ATPase 1 (Atp2b1) and 4 (Atp2b4) was detected. Similar expression of the voltage-dependent Ca^{2+} channel subunit alpha-2/delta-1 (Cacna2d1), a subunit that regulates Ca^{2+} current density and activation/inactivation kinetics of the Ca^{2+} channel, and the voltage-dependent L-type Ca^{2+} channel subunit beta-2 (Cacnb2) suggests similar Ca^{2+} influx in cardiomyocytes from $\alpha_2^{+/G301R}$ and WT mice. $n = 6$, except Atp2a3 and Atp2b4, where the signal was only detected in 3 WT and 3 $\alpha_2^{+/G301R}$ hearts. *, $P < 0.05$ (unpaired t -test). See also Data S1-S3.

Figure S9. Proteomics data analysis suggested that changed expression of Na,K-ATPase isoforms was associated with amplified Src/Ras/Erk1/2 signalling in hearts from 8-month-old $\alpha_2^{+/G301R}$ mice.

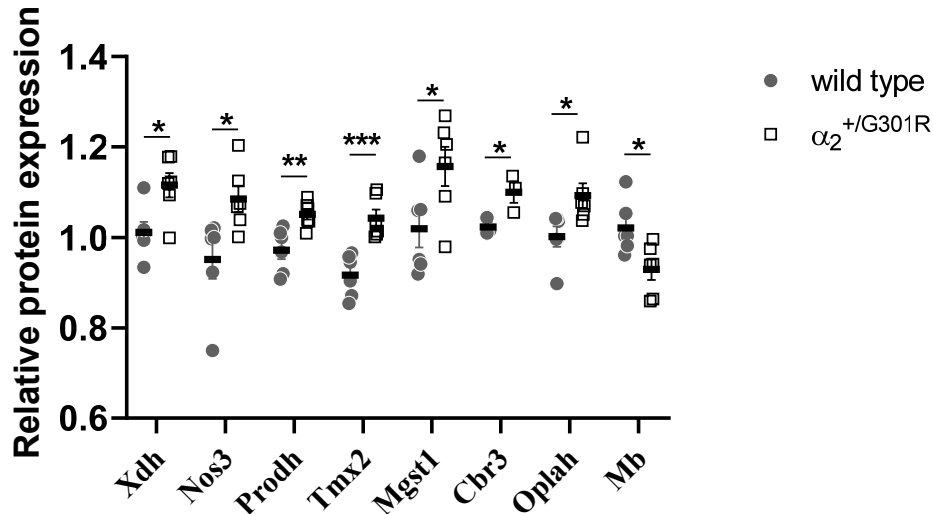


An increased expression of the Na,K-ATPase α_1 isoform and decreased expression of the α_2 isoform was detected by the proteomics data analysis in hearts from $\alpha_2^{+/G301R}$ mice (A). The $\alpha_2^{+/G301R}$ hearts had upregulated protein phosphatase 1 regulatory subunit 3A (Ppp1r3a), protein phosphatase 2 regulatory subunit B α (Ppp2r2a) and mitogen-activated protein kinase kinase 3 (Map2k3) suggesting increased signalling of the Src/Ras/Erk1/2 pathway (B). The Ras oncogene family members Rab4a, Rab11b and Rab14 were found upregulated, which further supported the finding of amplified Src/Ras/Erk1/2 signalling in the hearts from $\alpha_2^{+/G301R}$ mice (C). Interestingly, an increased expression of Rab4a was previously suggested to be responsible for hypersensitivity to β -adrenergic stimulation, metabolic remodelling and cardiac mitochondrial dysfunction.⁷⁶

$n = 6$. *, ** and ***, $P < 0.05$, < 0.01 and < 0.001 (unpaired t -test).

See also Data S1-S3.

Figure S10. Proteomics data analysis suggested upregulation of enzymes generating oxidative stress and enzymes involved in regulation of cellular redox state in the hearts from 8-month-old $\alpha_2^{+/G301R}$ mice.



Proteomics data analysis identified upregulation several enzymes known to contribute to generation of reactive oxygen species including xanthine oxidoreductase/dehydrogenase (Xdh),⁷⁷ nitric oxide synthase 3 (Nos3)⁷⁸ and proline dehydrogenase (Prodh).⁷⁹ An increased oxidative stress in the hearts of $\alpha_2^{+/G301R}$ mice was further supported by an increased expression of enzymes involved in regulation of cellular redox state, including thioredoxin related transmembrane protein 2 (Tmx2),⁸⁰ microsomal glutathione S-transferase 1 (Mgst1),⁸¹ carbonyl reductase 3 (Cbr3)⁸² and ATP-hydrolysing 5-oxoprolinase (Oplah).⁸³ Myoglobin (Mb), which acts as a short-term storage and reactive oxygen scavenger in cardiomyocytes,⁸⁴ was reduced in the hearts of $\alpha_2^{+/G301R}$ mice in comparison with wild type (WT).

$n = 6$, except Cbr3 where the signal was only detected in 3 WT and 3 $\alpha_2^{+/G301R}$ hearts.

*, ** and ***, $P < 0.05$, < 0.01 and < 0.001 (unpaired t -test). For reference, see also Data S1-S3.

Data S1.

Proteins mapped by proteomics of left ventricles from 8-month-old $\alpha_2^{+/G301R}$ and wild type mice.

Data compared using unpaired *t*-test.

Data S2.

Proteins relevant for the heart structure and function, which were significantly different between genotypes, suggested by Ingenuity Pathway Analysis of proteomics data from the hearts of 8-month-old $\alpha_2^{+/G301R}$ and wild type mice. Data compared using unpaired *t*-test.

Data S3.

The cardiac disease and altered function suggested by Ingenuity Pathway Analysis of proteomics data from the hearts of 8-month-old $\alpha_2^{+/G301R}$ and wild type mice. *P* values were calculated based on one-sided Fisher's exact test.

Data S4.

Whole uncropped Western blot gels

Data S4. Whole uncropped Western blot gels

Changed expression of the Na,K-ATPase α isoforms in the heart from $\alpha_2^{+/G301R}$ mice but similar expression of the Na,Ca-exchanger-1. Results are shown in Fig. 1.

A

3-month-old mice α_2 isoform of the Na,K-ATPase 8-month-old mice

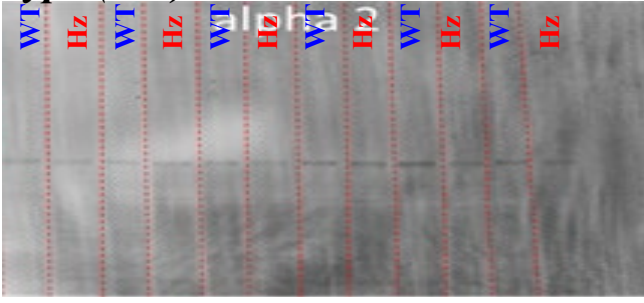
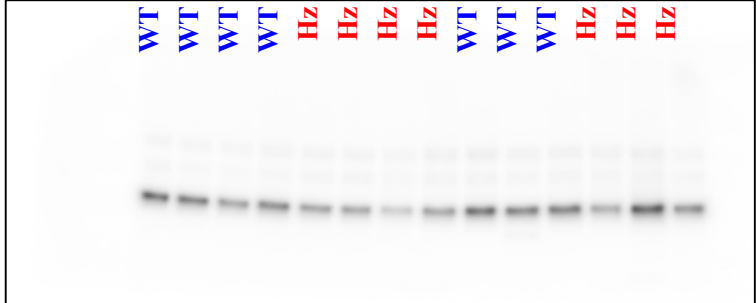
kDa:

Marker (kDa)

kDa:



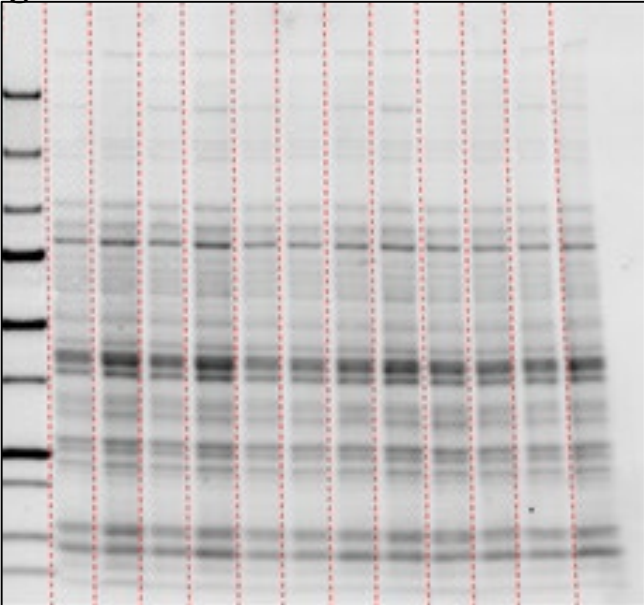
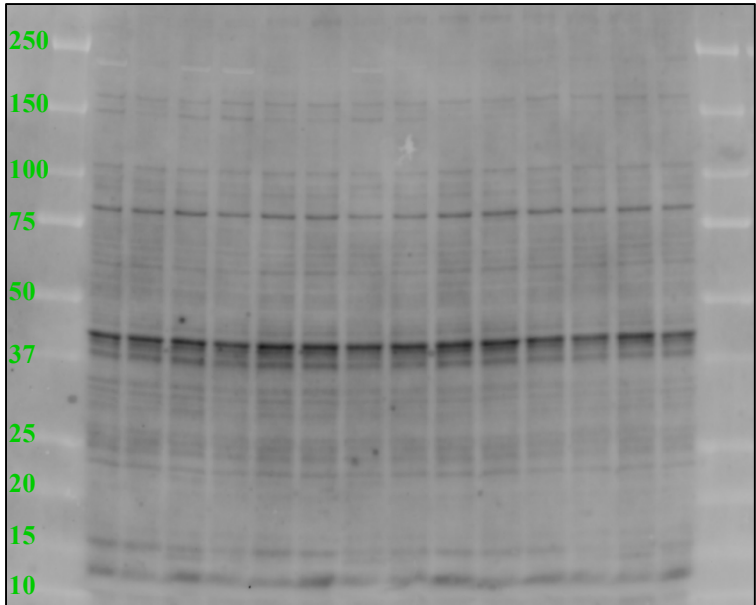
Western blot $\alpha_2^{+/G301R}$ (Hz) vs. wild type (WT)



Protein load , Stain-free gel

kDa:

kDa:



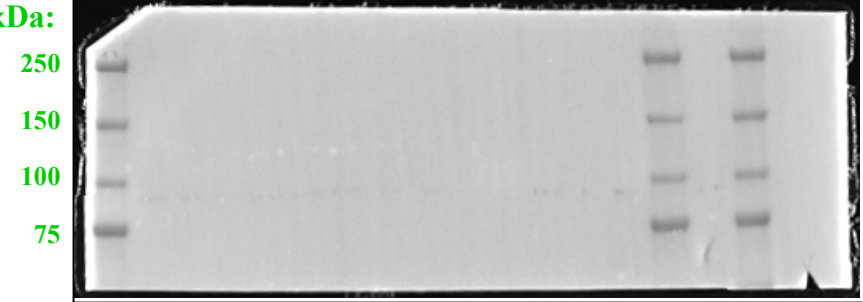
Changed expression of the Na,K-ATPase α isoforms in the heart from $\alpha_2^{+/G301R}$ mice but similar expression of the Na,Ca-exchanger-1. Results are shown in Fig. 1.

B

α_1 isoform of the Na,K-ATPase

3-month-old mice

8-month-old mice



Marker (kDa)

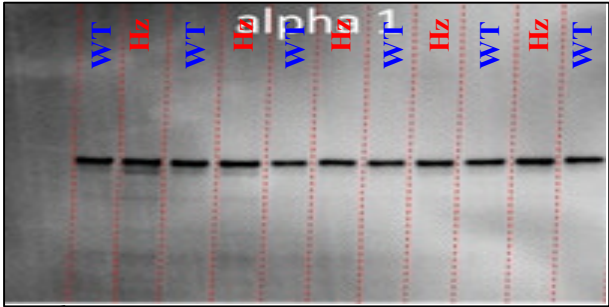
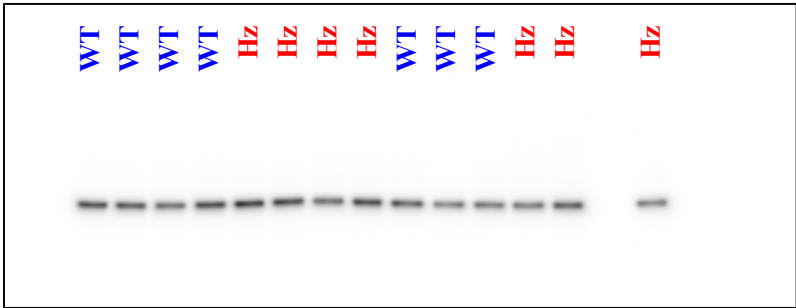
kDa: 250

150

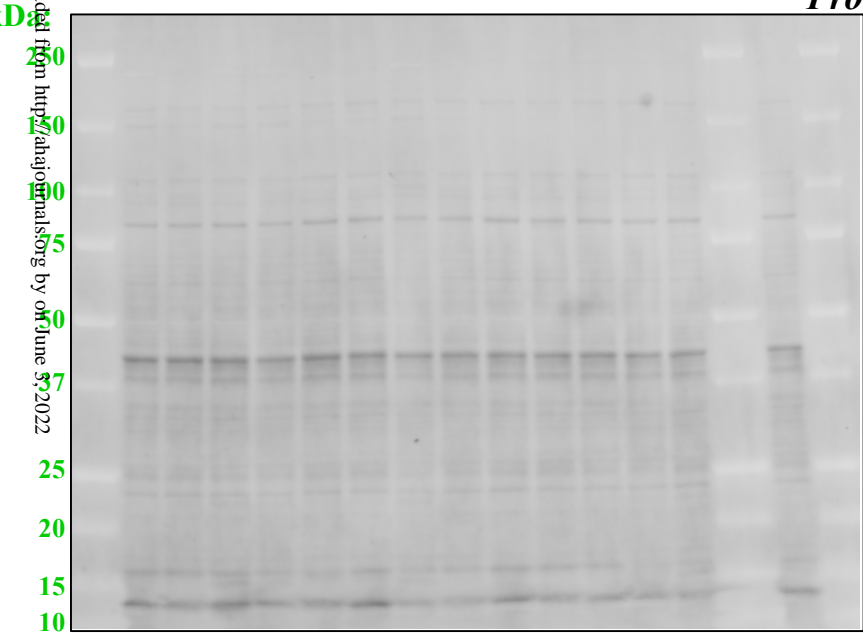
100

75

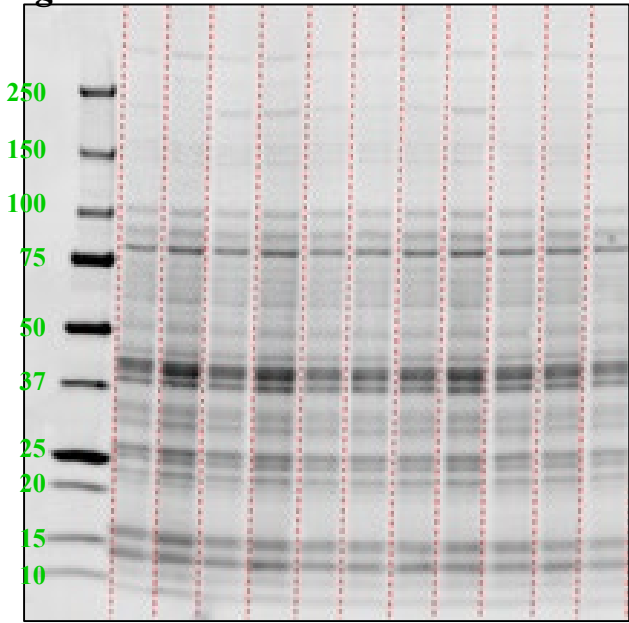
Western blot $\alpha_2^{+/G301R}$ (Hz) vs. wild type (WT)



Protein load, Stain-free gel



kDa:



C

Na,Ca-exchanger

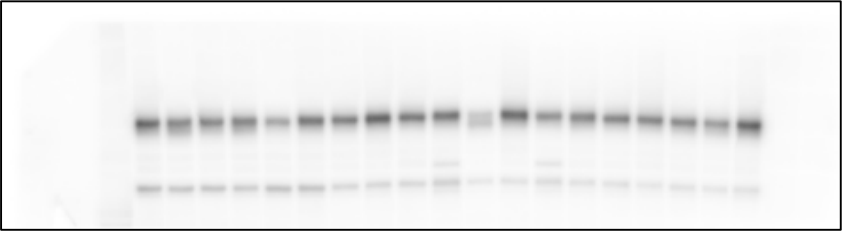
3-month-old (3-m) and 8-month-old (8-m) mice

Marker (kDa)

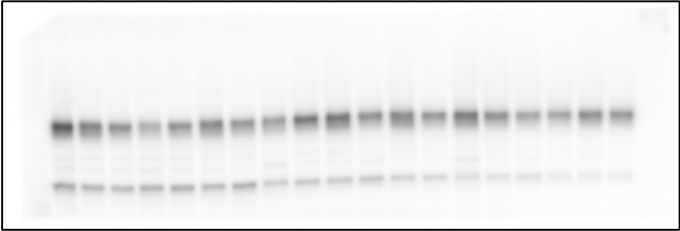


*Western blot $\alpha_2^{+/G301R}$ (**H**_z) vs. wild type (**W**_T)*

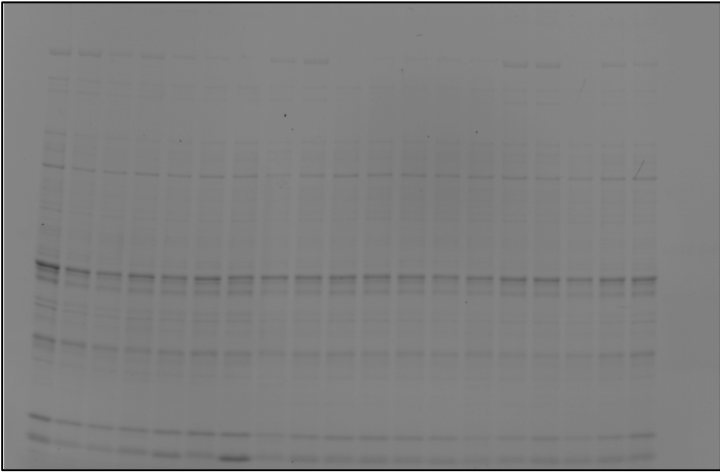
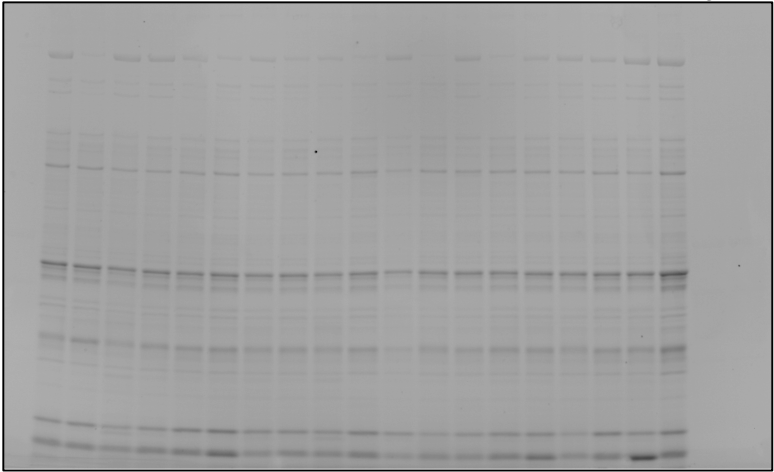
8-m 3-m 8-m 3-m 8-m 3-m 8-m 3-m 8-m 3-m 8-m 3-m 8-m 3-m 8-m 3-m 8-m 3-m



8-m 3-m 8-m 3-m 8-m 3-m 8-m 3-m 8-m 3-m 8-m 3-m 8-m 3-m 8-m 3-m 8-m 3-m

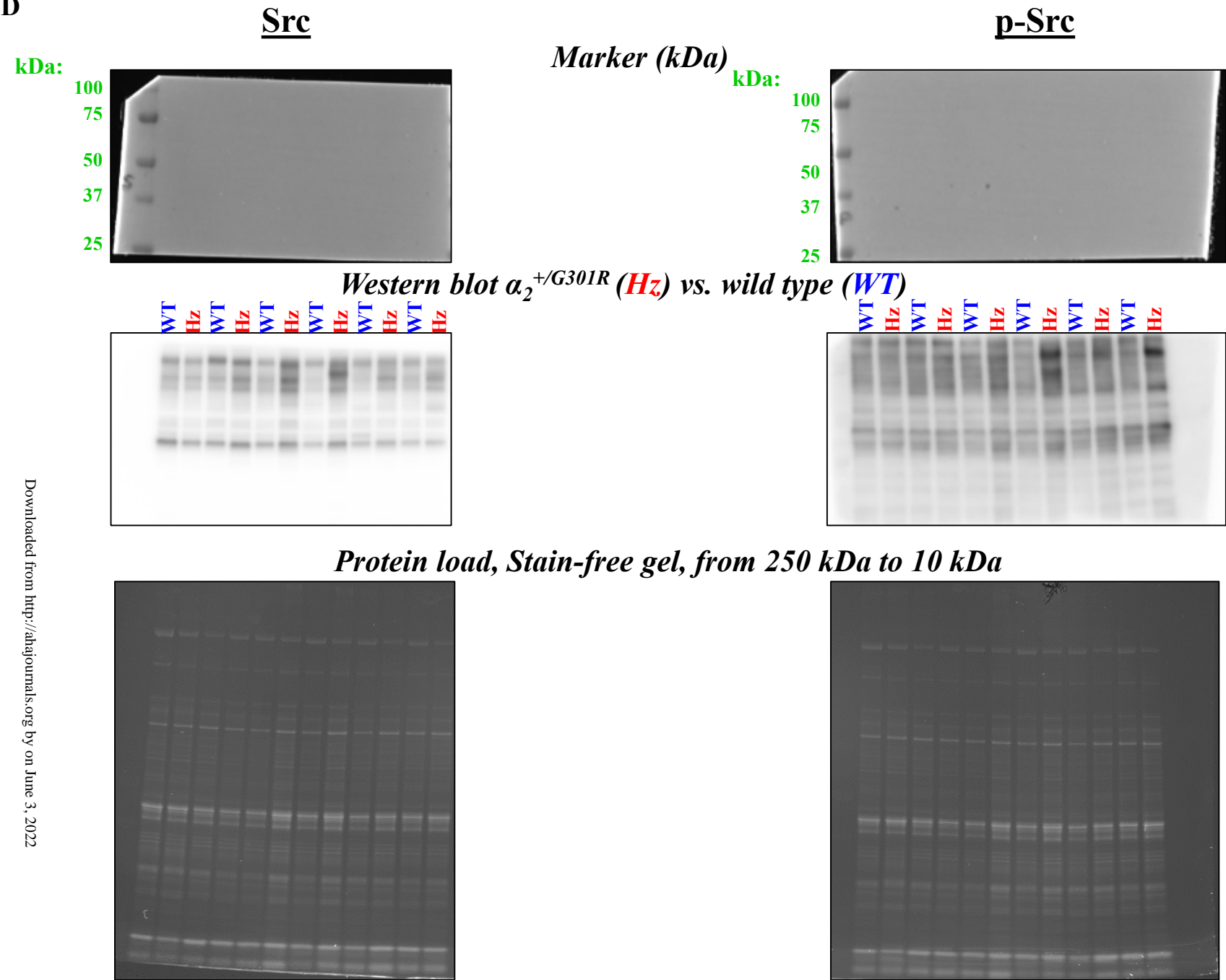


Protein load, Stain-free gel, from 250 kDa to 10 kDa



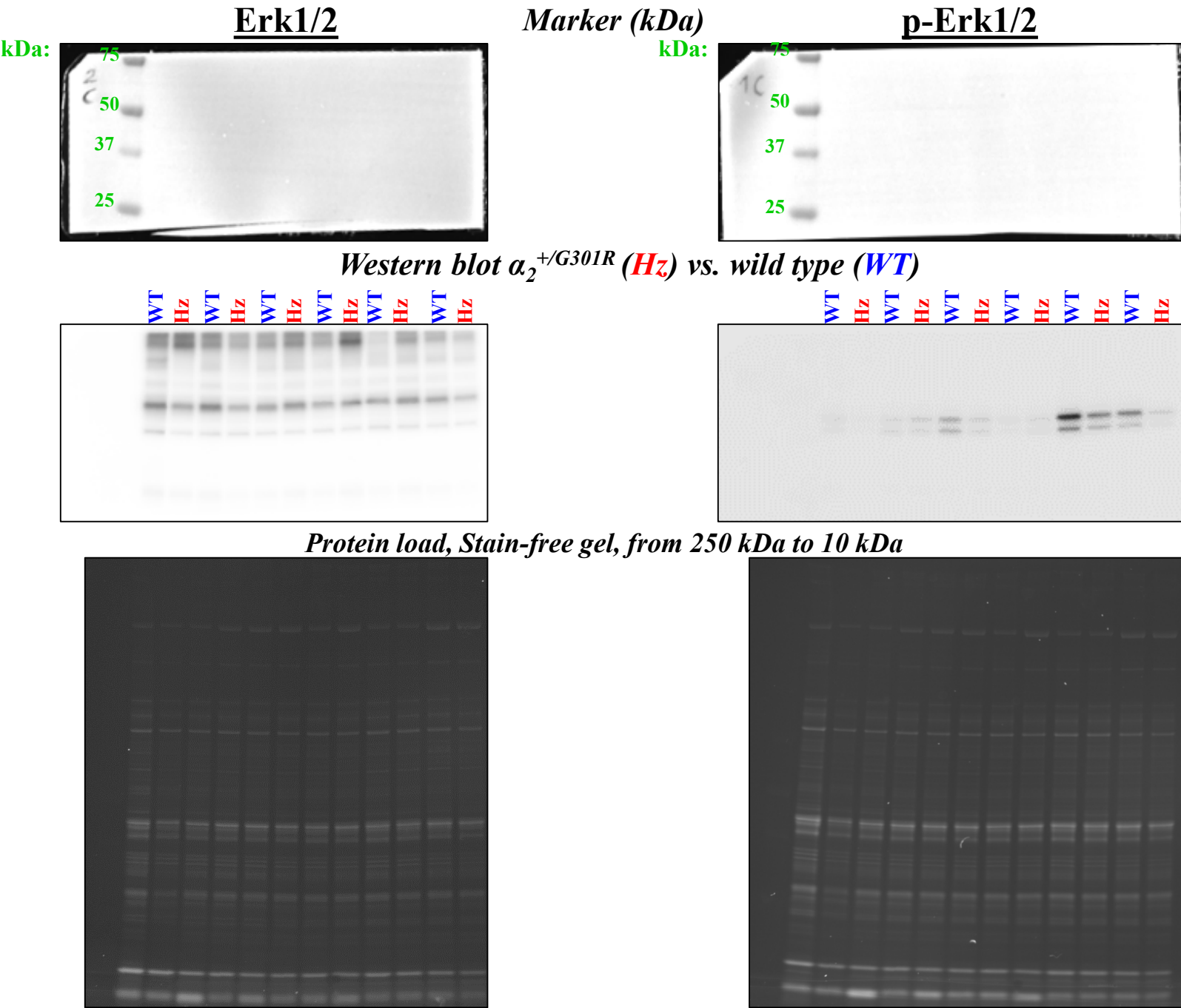
The hearts from 8-month-old $\alpha_2^{+/G301R}$ mice showed modified signalling of pathways downstream from the Na,K-ATPase. Results are shown in Fig. 6.

D



The hearts from 8-month-old $\alpha_2^{+/G301R}$ mice showed modified signalling of pathways downstream from the Na,K-ATPase. Results are shown in Fig. 6.

E



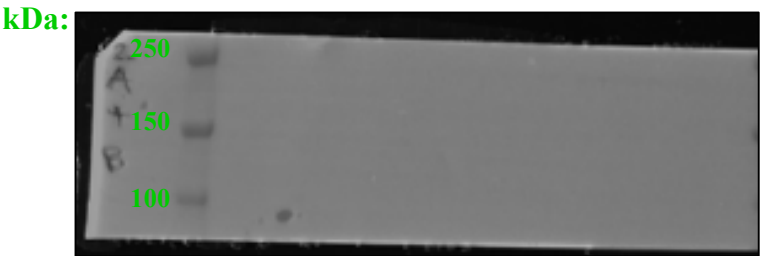
The hearts from 8-month-old $\alpha_2^{+/G301R}$ mice showed modified signalling of pathways downstream from the Na,K-ATPase. Results are shown in Fig. 6.

F

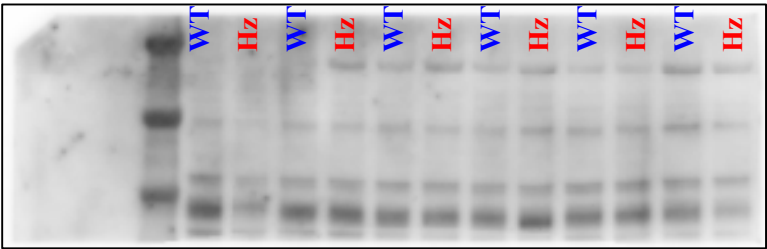
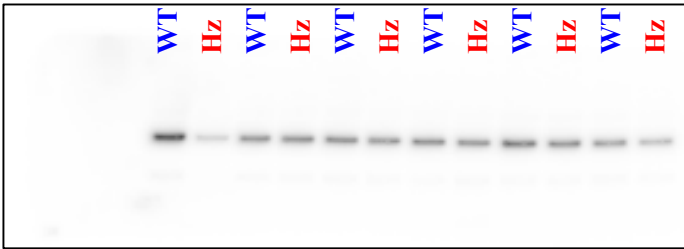
PLC γ

Marker (kDa)

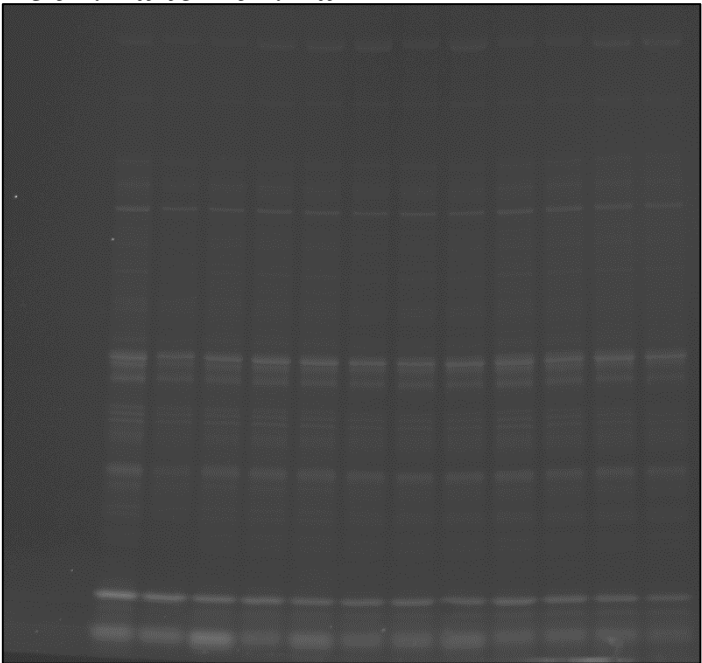
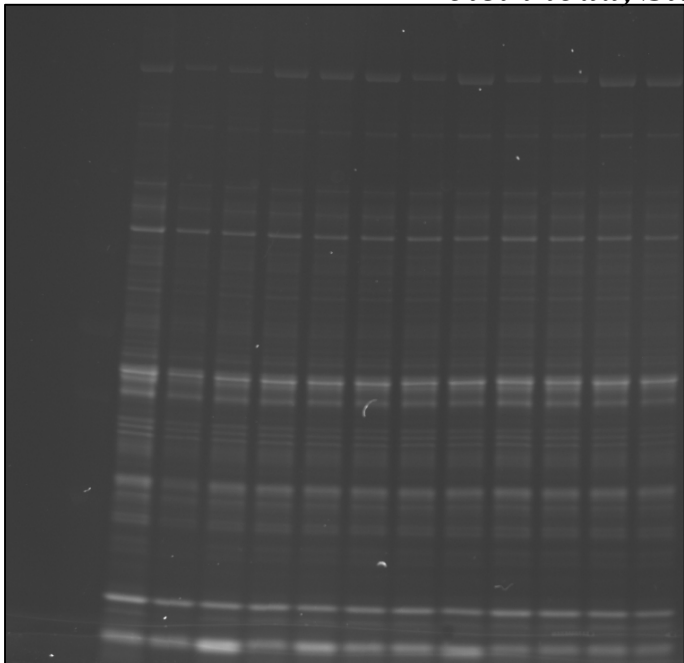
p-PLC γ



Western blot $\alpha_2^{+/G301R}$ (Hz) vs. wild type (WT)

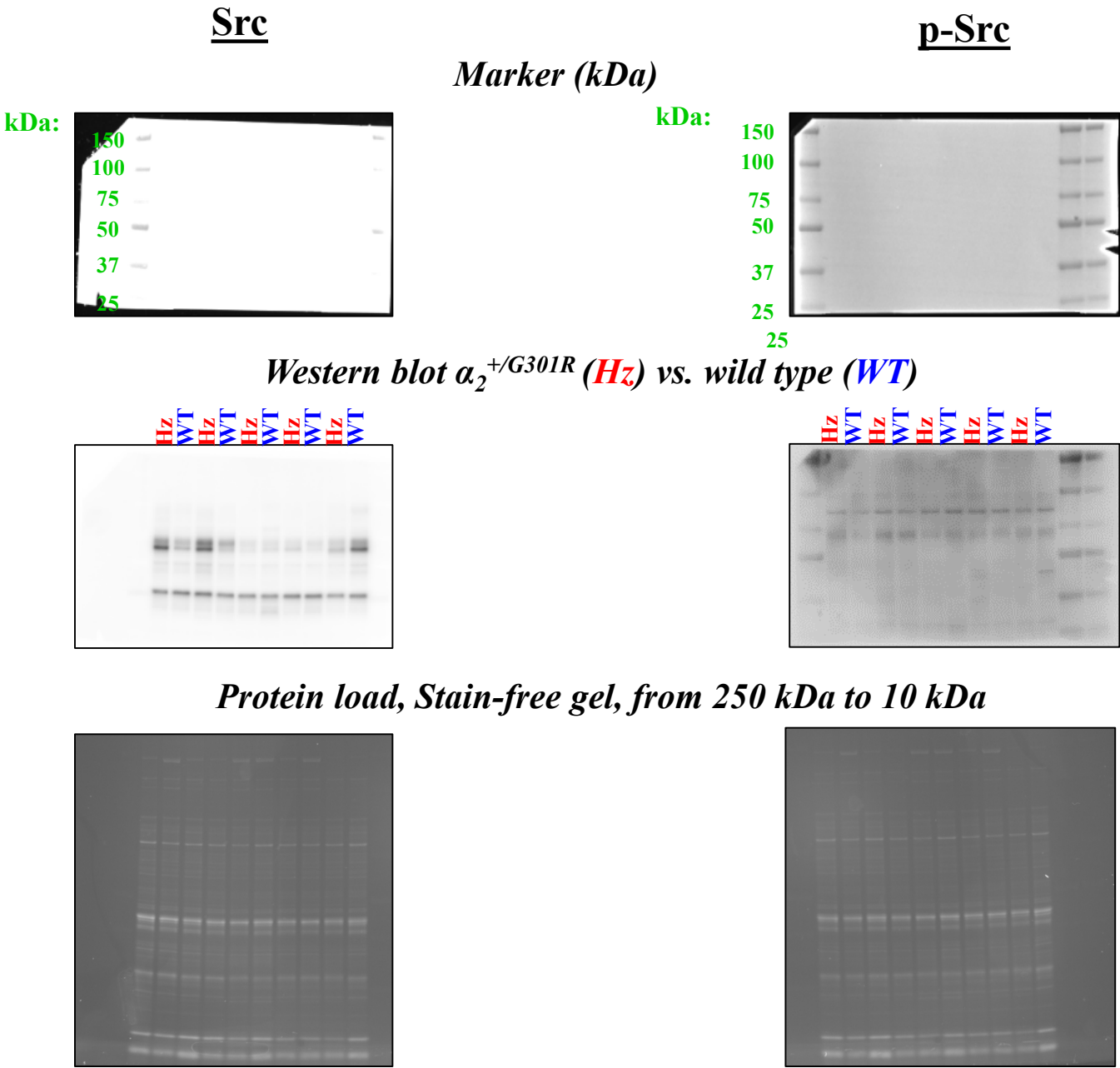


Protein load, Stain-free gel, from 250 kDa to 10 kDa



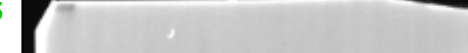
Phospho-specific Western blot analysis did not suggest any changes in the expression of key molecules for the Na,K-ATPase-dependent signalling pathways in the hearts from 3-month-old $\alpha_2^{+/G301R}$ and WT mice. Results are shown in Fig. S6.

G



Downloaded from <http://ahajournals.org> by on June 3, 2022

kDa: 75
50
37
25



kDa:

75

50

37

25

The image shows a portion of an SDS-PAGE gel. On the left side, molecular weight markers are indicated in kilodaltons (kDa) at 75, 50, 37, and 25. The gel itself is dark, and several horizontal bands representing proteins are visible. A prominent band is located between the 50 and 75 kDa markers, and another distinct band is visible just below the 37 kDa marker. There are also some fainter bands and smears throughout the gel.

[illegible][illegible]

Phospho-specific Western blot analysis did not suggest any changes in the expression of key molecules for the Na,K-ATPase-dependent signalling pathways in the hearts from 3-month-old $\alpha_2^{+/G301R}$ and WT mice. Results are shown in Fig. S6.

I

